

Momentum space treatment of inclusive neutrino scattering off the deuteron and trinucleons

J. Golak, R. Skibiński, K. Topolnicki, H. Witała, and A. Grassi

*M. Smoluchowski Institute of Physics,
Jagiellonian University, PL-30348 Kraków, Poland*

H. Kamada

*Department of Physics, Faculty of Engineering,
Kyushu Institute of Technology, Kitakyushu 804-8550, Japan*

L.E. Marcucci

*Department of Physics, University of Pisa,
IT-56127 Pisa, Italy and INFN-Pisa, IT-56127 Pisa, Italy*

(Dated: May 2, 2018)

Abstract

The $\bar{\nu}_e + {}^2\text{H} \rightarrow e^+ + n + n$, $\nu_e + {}^2\text{H} \rightarrow e^- + p + p$, $\bar{\nu}_l + {}^2\text{H} \rightarrow \bar{\nu}_l + {}^2\text{H}$, $\nu_l + {}^2\text{H} \rightarrow \nu_l + {}^2\text{H}$, $\bar{\nu}_l + {}^2\text{H} \rightarrow \bar{\nu}_l + p + n$, $\nu_l + {}^2\text{H} \rightarrow \nu_l + p + n$, $\bar{\nu}_e + {}^3\text{He} \rightarrow e^+ + {}^3\text{H}$, $\bar{\nu}_l + {}^3\text{He} \rightarrow \bar{\nu}_l + {}^3\text{He}$, $\nu_l + {}^3\text{He} \rightarrow \nu_l + {}^3\text{He}$, $\bar{\nu}_l + {}^3\text{H} \rightarrow \bar{\nu}_l + {}^3\text{H}$, $\nu_l + {}^3\text{H} \rightarrow \nu_l + {}^3\text{H}$, $\bar{\nu}_e + {}^3\text{He} \rightarrow e^+ + n + d$, $\bar{\nu}_e + {}^3\text{He} \rightarrow e^+ + n + n + p$, $\bar{\nu}_l + {}^3\text{He} \rightarrow \bar{\nu}_l + p + d$, $\bar{\nu}_l + {}^3\text{He} \rightarrow \bar{\nu}_l + p + p + n$, $\nu_l + {}^3\text{H} \rightarrow \nu_l + n + d$ and $\nu_l + {}^3\text{H} \rightarrow \nu_l + n + n + p$ reactions ($l = e, \mu, \tau$) are studied consistently in momentum space for (anti)neutrino energies up to 300 MeV. For most of these processes we provide predictions for the total cross sections and in the case of the (anti)neutrino- ${}^3\text{He}$ and (anti)neutrino- ${}^3\text{H}$ inelastic scattering we compute examples of essential response functions, using the AV18 nucleon-nucleon potential and a single-nucleon weak current operator. For the reactions with the deuteron we study relativistic effects in the final state kinematics and compare two-nucleon scattering states obtained in momentum and coordinate spaces. Our results from momentum space are compared with the theoretical predictions by G. Shen *et al.*, Phys. Rev. C **86**, 035503 (2012). The observed disagreement can be attributed to the differences in kinematics and in the weak current operator.

PACS numbers: 23.40.-s, 21.45.-v, 27.10.+h

I. INTRODUCTION

Neutrino scattering on nuclei has been studied for several decades. For information on the status of earlier theoretical treatments of neutrino-nucleus reactions, relevant to the detection of astrophysical neutrinos, we refer the reader to Ref. [1]. At the beginning of the century theoretical work was motivated by the establishment of the Sudbury Neutrino Observatory and resulted in important predictions by Nakamura *et al.* [2, 3]. They calculated cross sections for both charged-current (CC) and neutral-current (NC) driven reactions, for incoming neutrino energies up to 150 MeV. The results of Ref. [2] and the bulk of predictions given in Ref. [3] were obtained within the so-called "standard nuclear physics approach" [4], employing the AV18 nucleon-nucleon (NN) force [5] and supplementing the single-nucleon current with two-nucleon (2N) current contributions related to this potential. Some calculations in Ref. [3] were done with the CD-Bonn NN potential [6] or using input from chiral effective field theory (χ EFT) in order to estimate theoretical uncertainties of the results, which were later used to analyze experimental data from the Sudbury Neutrino Observatory [7].

More recent calculations by Shen *et al.* [8] were also done within the traditional approach, using the AV18 potential and corresponding nuclear weak current operators with a one-body part and two-body contributions, adjusted to the NN force. The authors of Ref. [8] studied inclusive neutrino scattering on the deuteron up to neutrino energies of 1 GeV with configuration space methods. Although they introduced some changes in the 2N current operator used by Nakamura *et al.*, these modifications proved to be of minor importance and the results obtained by Shen *et al.* confirmed those of Nakamura *et al.* in the energy range up to 150 MeV. Conclusions presented in Ref. [8] provided important information on the role of 2N currents and final state interaction effects for the whole considered neutrino energy range, even though pion production channels were neglected.

Despite the successes achieved within the traditional approach, new calculations emerging from χ EFT offered competitive results. Already in 2001 Butler *et al.* [9] studied the neutrino-deuteron break-up reactions at next-to-next-to-leading order (N2LO) in pionless χ EFT, in the energy range up to 20 MeV. Their work agreed very well with the previous potential model calculations from Refs. [2, 3].

Attempts to build a complete theoretical framework comprising consistent "chiral" 2N and many-nucleon forces as well as electroweak current operators at a sufficiently high order of the chiral expansion have a long history. A construction of the chiral NN potential was pioneered by Weinberg [10, 11] almost thirty years ago and developed by several groups. In particular Epelbaum *et al.* have prepared three generations of the chiral potentials. They started with the version of the NN potential, where the non-local regularization in momentum space was implemented [12–14]. They derived also the widely used chiral three-nucleon (3N) potential at N2LO [15], summarizing the work on chiral forces and their applications to processes involving few nucleons up to 2005 in Ref. [16]. Further important contributions from this group dealt with the 3N force at next-to-next-to-next-to-leading order (N3LO) [17, 18], the four-nucleon force [19], and a formulation of the Δ -full chiral perturbation theory [20, 21].

The next generation of the chiral NN potential by Epelbaum *et al.* used a coordinate space regularization. This improved version from Refs. [22, 23] led to a significant reduction of finite-cutoff artefacts, did not require any additional spectral function regularization and directly employed low-energy constants determined from pion-nucleon scattering. These

forces were used to study nucleon-deuteron scattering [24] and various electroweak processes in 2N and 3N systems [25].

The newest version of the Bochum-Bonn chiral NN potential, prepared up to fifth order in the chiral expansion (N4LO), was introduced very recently in Ref. [26]. Important changes include a removal of the redundant contact terms and regularization in momentum space, resulting in an excellent description of the proton-proton and neutron-proton scattering data from the self-consistent Granada-2013 database [27].

The Bochum-Bonn group has also been working on the chiral electromagnetic [28, 29] and weak (axial) [30] current operators. First results with the 2N electromagnetic currents from Ref. [28] were published in Refs. [31, 32], but full-fledged calculations with the consistent Bochum-Bonn potentials and current operators will become possible, when the ongoing work on the regularization of the current operators is completed.

Concurrent with these studies have been the efforts by the Moscow(Idaho)-Salamanca group, which resulted in another family of non-local chiral NN potentials [33, 34]. The most recent version of this potential, generated also up to fifth order in the chiral expansion was published in Ref. [35]. At N4LO it reproduces the world NN data with the χ^2/datum of 1.08 for proton-proton and neutron-proton data up to 190 MeV.

Many modern calculations of various electromagnetic processes employ the chiral potentials from Refs. [33, 34] and require chiral current operators. The latter were developed gradually, starting with a pioneering work by Park *et al.* [36]. The predictions of Refs. [36, 37] were later re-derived or supplemented by many authors [38–41], using various formulations of χEFT . The unknown parameters of the effective theory were either related to the NN scattering or fixed by reproducing selected observables in the 2N and 3N systems, like the magnetic moments [42] and the tritium Gamow-Teller matrix element [43, 44]. The derived current operators were used with the wave functions obtained with the traditional potentials and later, more consistently, with the potentials derived by the Moscow(Idaho)-Salamanca group. Among the many studied processes were those of direct astrophysical interest [45, 46], muon capture reactions [47–50] and, last but not least, neutrino induced processes [51].

Predictions in Ref. [51] for inclusive neutrino scattering off the deuteron are fully based on a χEFT input. The results concerning the cross sections are only slightly larger than the corresponding ones obtained in conventional formulations based on meson-exchange picture [3, 8] and are insensitive to the value of the regulator parameter. This might indicate that the theoretical results have a very small uncertainty in the low-energy neutrino regime.

To give the reader a proper picture of the efforts aiming at the exact treatment of the neutrino induced reactions, we mention here some calculations with heavier than $A = 2$ nuclei. Gazit *et al.* performed a number of calculations for neutrino induced break-up reactions with the ^3H , ^3He and ^4He nuclei [52–54], in which final state interactions were included via the Lorentz integral transform method [55]. The resulting bound-state and bound-state-like equations were solved using the effective interaction hyperspherical harmonics (EIHH) approach [56, 57], employing conventional 2N and 3N forces. While in Ref. [52] the impulse approximation was used, in Refs. [53, 54] the nuclear current operator contained also 2N contributions derived from χEFT . Finally, we mention that weak inclusive responses of heavier light nuclei, including ^{12}C , were investigated with the Green’s function Monte Carlo method [58, 59]. The results of these calculations contributed to the determination of the nucleon isovector axial form factor [60].

The momentum-space approach offers an independent possibility to perform calculations not only for the deuteron but also for the trinucleons’ reactions with neutrinos. In the present

work we calculate cross sections for several such reactions and build a solid base upon which we can improve our dynamics in the future, adding many-nucleon forces and weak current operators. The present study, contrary to the very advanced investigations by Baroni *et al.* [51], is carried out with rather simple dynamical input. Namely we work with the traditional AV18 NN potential and restrict ourselves to the single nucleon current. Thus we definitely cannot reach yet the high level of accuracy achieved by the predictions of Refs. [3, 8, 51], dealing solely with the neutrino induced break-up of ${}^2\text{H}$. We agree with the statement in Ref. [51] that the accuracy of these predictions is very important in the analysis of the SNO experiments and more generally for our understanding of (anti)neutrino-nucleus scattering. Thus we decided to confront our momentum-space framework predictions with the above-mentioned results. We also agree with Ref. [51] that all these ingredients should be derived consistently from χEFT . There are, however, still some open issues in the construction of the 2N electroweak current operator and the results for the axial current obtained by Krebs *et al.* [30] are not equivalent to those reported in Refs. [41, 44]. Even if these differences prove to be of no practical importance, some fundamental questions about the consistence between chiral potentials and current operators still should be answered. Our framework is anyway ready for the improved input generated by χEFT .

The results obtained within χEFT are usually provided in momentum space and can be readily incorporated in momentum-space calculations. We refer the reader especially to the so-called "three-dimensional" calculations, which avoid totally partial wave representation of nuclear states and operators [61, 62]. In this approach χEFT potentials and current operators would be used indeed directly, avoiding also convergence problems bound with partial wave decomposition. Our present results might thus provide a benchmark for such planned calculations.

Last but not least, momentum space framework allows one to systematically account for relativistic effects not only in the kinematics but also in the reaction dynamics. Some of such problems might be difficult to tackle in coordinate space but are easier to solve in momentum space. For example, the argument of the nucleon form factors in the single-nucleon current, which should be actually the four-momentum transfer *to the nucleon* squared, is usually replaced by the four-momentum transfer *to the whole nuclear system* squared. In momentum space one can directly use the proper values of the form factor arguments.

Relativity plays definitely an important role for higher neutrino energies. Even at relatively low energies these effects have to be studied thoroughly, since approximate treatment of relativity adds to the total theoretical uncertainty of predictions. Ultimately, theoretical calculations should take into account complementary roles of kinematic and dynamical contributions to the Poincaré invariant formulation of reaction theory. Important examples of such investigations are given in Refs. [63–69]. A particular result of these studies, showing that relativistic effects in kinematics and dynamics might in fact partly cancel, prompted us to retain the nonrelativistic form of the phase space factor, consistent with our nonrelativistic dynamics, in particular with the form of the current operator. Consequences of this choice will be discussed below.

The paper is organized in the following way. In Sec. II we introduce elements of our formalism and compare it with the calculations presented in Refs. [2, 8]. In particular we discuss the differences in the treatment of kinematics and the current operator. In the following two sections we show selected results for various processes induced by neutrinos. Finally, Sec. V contains some concluding remarks and outlook.

II. ELEMENTS OF THE FORMALISM

Recently we have developed a framework to study several muon capture processes on the ${}^2\text{H}$, ${}^3\text{H}$ and ${}^3\text{H}$ nuclei [62, 70]. For the $\bar{\nu}_l + {}^2\text{H} \rightarrow l^+ + n + n$ reaction, the transition from the initial to final state is also governed by the Fermi form of the interaction Lagrangian [71], again leading to a contraction of the leptonic (\mathcal{L}_λ) and nuclear (\mathcal{N}^λ) parts in the S matrix element, S_{fi} :

$$S_{fi} = i(2\pi)^4 \delta^4(P' - P) \frac{G_F \cos \theta_C}{\sqrt{2}} \mathcal{L}_\lambda \mathcal{N}^\lambda, \quad (2.1)$$

where the value of the Fermi constant, $G_F = 1.1803 \times 10^{-5} \text{ GeV}^{-2}$, and $\cos \theta_C = 0.97425$ have been deliberately taken to be the same as in Ref. [8]. The total initial (final) four-momentum is denoted as P (P').

The leptonic matrix element

$$\mathcal{L}_\lambda = \frac{1}{(2\pi)^3} \bar{v}(\mathbf{k}, m_{\bar{\nu}}) \gamma_\lambda (1 - \gamma_5) v(\mathbf{k}', m_{l^+}) \equiv \frac{1}{(2\pi)^3} L_\lambda \quad (2.2)$$

is given in terms of the Dirac spinors v and the gamma matrices [72], and depends on the initial antineutrino three-momentum \mathbf{k} and spin projection $m_{\bar{\nu}}$ as well as on the final antilepton three-momentum \mathbf{k}' and spin projection m_{l^+} . The same formula holds for the three lepton flavors $l = e$, $l = \mu$ and $l = \tau$.

The nuclear part

$$\mathcal{N}^\lambda = \frac{1}{(2\pi)^3} \langle \Psi_f \mathbf{P}_f m_f | j_{CC}^\lambda | \Psi_i \mathbf{P}_i m_i \rangle \equiv \frac{1}{(2\pi)^3} N_{CC}^\lambda \quad (2.3)$$

is a matrix element of the nuclear weak charged current (CC) operator j_{CC}^λ between the initial and final nuclear states. The total initial (final) nuclear three-momentum is denoted as \mathbf{P}_i (\mathbf{P}_f), m_i is the initial nucleus spin projection and m_f is the set of spin projections in the final state. In this paper we restrict ourselves to the single nucleon current operator with relativistic corrections. This current operator was described in detail in Ref. [62]. It is very close to the one used in Ref. [48] and employs form factors, whose explicit expressions and parametrization can be found in Ref. [8].

On top of the single nucleon operators, also many-nucleon contributions appear in j_{CC}^λ . Their role has been studied for example in Ref. [48]. For the neutrino induced reactions of interest, the effects of 2N contributions in the weak current operator were estimated in Ref. [8] to be smaller than 10% over the wide energy range from the threshold to GeV energies. Thus we decided to base our first predictions on the single nucleon current only and represent all dynamical ingredients in momentum space.

The only change in the charged single nucleon current operator for the $\nu_l + {}^2\text{H} \rightarrow l^- + p + p$ process compared to the $\bar{\nu}_l + {}^2\text{H} \rightarrow l^+ + n + n$ reaction is the replacement of the overall isospin lowering operator by the isospin raising operator:

$$\tau_- \equiv (\tau_x - i\tau_y)/2 \longrightarrow \tau_+ \equiv (\tau_x + i\tau_y)/2. \quad (2.4)$$

However, since the matrix elements of the single nucleon operator in the 2N isospin space, spanned by the $|(\frac{1}{2}\frac{1}{2})tm_t\rangle$ states, $\langle(\frac{1}{2}\frac{1}{2})1-1|\tau_-(1)|(\frac{1}{2}\frac{1}{2})00\rangle$ and $\langle(\frac{1}{2}\frac{1}{2})11|\tau_+(1)|(\frac{1}{2}\frac{1}{2})00\rangle$ have just an opposite sign, we can use for this reaction *exactly* the same single

nucleon current operator. Its matrix elements, N_{CC}^λ , are contracted with the altered leptonic matrix elements

$$L_\lambda = \bar{u}(\mathbf{k}', m_{l^-}) \gamma_\lambda (1 - \gamma_5) u(\mathbf{k}, m_\nu), \quad (2.5)$$

expressed through the Dirac spinors u , which depend on the initial neutrino three-momentum \mathbf{k} and spin projection m_ν , as well as on the final lepton three-momentum \mathbf{k}' and spin projection m_{l^-} . In the following the energy of the initial (anti)neutrino will be denoted by E and for the massless (anti)neutrino $E = |\mathbf{k}|$.

A. Kinematics

Since we compare our purely nonrelativistic predictions with the ones published in Ref. [8], where the relativistic kinematics was employed, we give here formulas for our kinematics and cross sections for all studied reactions. We believe that they will be useful in the future benchmark calculations and serve to disentangle relativistic kinematical effects from dynamical ones. The difference in the treatment of kinematics is the main reason, why our predictions diverge from the results published in Ref. [8], especially for higher energies.

The kinematics of the $\bar{\nu}_l + {}^2\text{H} \rightarrow l^+ + n + n$ and $\nu_l + {}^2\text{H} \rightarrow l^- + p + p$ processes is essentially identical (the only difference being the mass of two identical nucleons in the final state) and can be treated both relativistically and nonrelativistically. The relativistic formulas for different kinematical quantities are given in Refs. [2, 8], so we can focus on the differences between the exact relativistic and our approximate nonrelativistic treatment of kinematics.

The starting point is the energy and momentum conservation, where we neglect the very small (anti)neutrino mass and assume that the initial deuteron is at rest. In the relativistic formalism it reads:

$$\begin{aligned} E + M_d &= \sqrt{M_l^2 + \mathbf{k}'^2} + \sqrt{M_p^2 + \mathbf{p}_1^2} + \sqrt{M_p^2 + \mathbf{p}_2^2}, \\ \mathbf{k} &= \mathbf{k}' + \mathbf{p}_1 + \mathbf{p}_2. \end{aligned} \quad (2.6)$$

Here \mathbf{p}_1 and \mathbf{p}_2 stand for the individual momenta of the two outgoing nucleons. The deuteron, nucleon and (anti)lepton masses are denoted as M_d , M_p and M_l , respectively. In the nonrelativistic version of Eqs. (2.6) we replace the first equation by

$$E + M_d = \sqrt{M_l^2 + \mathbf{k}'^2} + 2M_p + \frac{\mathbf{p}_1^2}{2M_p} + \frac{\mathbf{p}_2^2}{2M_p}, \quad (2.7)$$

using nonrelativistic formulas in the nuclear sector. We make sure to what extent the nonrelativistic approximation is justified by comparing values of various quantities calculated nonrelativistically and using relativistic equations. This is important, since our dynamics is entirely nonrelativistic.

We begin with the (anti)neutrino threshold energy, E_{thr} . Relativistically, the condition for the total energy of the system in the zero-momentum frame

$$(E + M_d)^2 - \mathbf{k}^2 \geq (M_l + 2M_p)^2 \quad (2.8)$$

leads to

$$E \geq E_{thr}^{rel} \equiv \frac{(M_l + 2M_p)^2 - M_d^2}{2M_d}. \quad (2.9)$$

TABLE I. Threshold energies in MeV for various (anti)neutrino induced reactions on the deuteron calculated relativistically (E_{thr}^{rel}) and using two nonrelativistic prescriptions (E_{thr}^{nrl} and \mathcal{E}_{thr}^{nrl}). We assumed $M_d = 1875.613$ MeV, $M_p = 938.272$ MeV, $M_n = 939.565$ MeV and $M_e = 0.510999$ MeV. Results for the $\nu_l + d \rightarrow \nu_l + p + n$ and $\bar{\nu}_l + d \rightarrow \bar{\nu}_l + p + n$ processes are identical.

| reaction | E_{thr}^{rel} | E_{thr}^{nrl} | \mathcal{E}_{thr}^{nrl} |
|---|-----------------|-----------------|---------------------------|
| $\bar{\nu}_e + d \rightarrow e^+ + n + n$ | 4.03323 | 4.03323 | 4.03323 |
| $\nu_e + d \rightarrow e^- + p + p$ | 1.44279 | 1.44279 | 1.44279 |
| $\nu_l + d \rightarrow \nu_l + p + n$ | 2.22589 | – | 2.22589 |

In the fully nonrelativistic approach, one treats even the final (anti)lepton nonrelativistically and obtains

$$E + M_d = M_l + 2M_p + \frac{\mathbf{k}'^2}{2M_l} + \frac{\mathbf{p}_1^2}{2M_p} + \frac{\mathbf{p}_2^2}{2M_p} \equiv M_l + 2M_p + T_{lab}, \quad (2.10)$$

where T_{lab} is the total kinetic energy in the laboratory frame. Then the threshold energy is obtained from the condition that the kinetic energy calculated in the center of mass frame, T_{cm} , is non-negative:

$$T_{cm} = T_{lab} - \frac{\mathbf{k}^2}{2(M_l + 2M_p)} \geq 0 \quad (2.11)$$

and reads

$$E_{thr}^{nrl} = M_l + 2M_p - \sqrt{(M_l + 2M_p)(2M_d - M_l - 2M_p)}. \quad (2.12)$$

Actually this result does not follow from Eq. (2.7), where we apply the nonrelativistic formulas only to the outgoing nucleons. In order to be consistent, we rewrite Eq. (2.7) as

$$E + M_d = \sqrt{M_l^2 + \mathbf{k}'^2} + 2M_p + \frac{\mathbf{p}_{12}^2}{4M_p} + \frac{\mathbf{p}^2}{M_p}, \quad (2.13)$$

where $\mathbf{p}_{12} \equiv \mathbf{p}_1 + \mathbf{p}_2 = \mathbf{k} - \mathbf{k}'$ and $\mathbf{p} = \frac{1}{2}(\mathbf{p}_1 - \mathbf{p}_2)$. Next we numerically seek the smallest possible value of E (represented by \mathcal{E}_{thr}^{nrl}), for which a physical solution of

$$E + M_d = \sqrt{M_l^2 + \mathbf{k}'^2} + 2M_p + \frac{(\mathbf{k} - \mathbf{k}')^2}{4M_p} \quad (2.14)$$

exists.

Obviously the same logic applies to the $\nu_l + d \rightarrow \nu_l + p + n$ and $\bar{\nu}_l + d \rightarrow \bar{\nu}_l + p + n$ reactions. In this case the relativistic result is still exact, but in the nonrelativistic calculations we additionally neglect the small difference between the proton mass M_p and neutron mass M_n and use the average ‘‘nucleon mass’’, $M \equiv \frac{1}{2}(M_p + M_n)$. For the massless particle in the final state, the fully nonrelativistic calculation is not possible. From Table I, where we display all the numerical results for the threshold energies, it is clear that difference between the relativistic and nonrelativistic results are insignificant.

Next, we determine the maximal energy of the emerging lepton under a given scattering angle θ , where $\cos \theta = \hat{\mathbf{k}} \cdot \hat{\mathbf{k}'}$. Note that there is no restriction on the scattering angle

θ . Relativistically, we set the condition for the total energy of two nucleons in their zero-momentum frame

$$\left(E + M_d - \sqrt{M_l^2 + \mathbf{k}'^2}\right)^2 - (\mathbf{k} - \mathbf{k}')^2 \geq 4M_p^2. \quad (2.15)$$

Simple algebra leads just to a quadratic inequality for $k' \equiv |\mathbf{k}'|$:

$$\begin{aligned} & (4(E + M_d)^2 - 4E^2 \cos^2 \theta) k'^2 \\ & + (-4E(2EM_d + M_d^2 + M_l^2 - 4M_p^2) \cos \theta) k' \\ & + 4(E + M_d)^2 M_l^2 - (2EM_d + M_d^2 + M_l^2 - 4M_p^2)^2 \leq 0 \end{aligned} \quad (2.16)$$

and the bigger of the two roots of the corresponding quadratic equation is the maximal value of the magnitude of the outgoing lepton, $(k')_{max}^{rel}$.

In the nonrelativistic approximation the kinetic energy of the 2N system in the 2N total momentum zero frame must be non-negative:

$$E + M_d - 2M_p - \sqrt{M_l^2 + \mathbf{k}'^2} - \frac{(\mathbf{k} - \mathbf{k}')^2}{4M_p} \geq 0. \quad (2.17)$$

This condition yields now a fourth degree equation:

$$\begin{aligned} & k'^4 - 4E \cos \theta k'^3 \\ & + (4E^2 \cos^2 \theta - 16M_p^2 - 2W) k'^2 \\ & + 4WE \cos \theta k' + W^2 - 16M_p^2 M_l^2 = 0, \end{aligned} \quad (2.18)$$

with $W \equiv 4M_p(E + M_d - 2M_p) - E^2$. One of the roots of Eq. (2.18) is the nonrelativistic analogue of $(k')_{max}^{rel}$, which we denote by $(k')_{max}^{nrl}$. Its values are found numerically, starting the search from $(k')_{max}^{rel}$. In Fig. 1 we show a comparison of the kinematical constraints for $(k')_{max}$, comparing $(k')_{max}^{rel}$ and $(k')_{max}^{nrl}$ for two initial electron neutrino energies, $E=150$ and 300 MeV. Even at $E=300$ MeV curves representing two different results nearly overlap. The maximal difference is noticed for the backward angles, but it does not reach 0.5 %.

The last issue we want to discuss here concerns the phase space factor. In Refs. [2, 8] two different relativistic forms are employed. Since in Ref. [8] the same variables are used as in our nonrelativistic framework, we focus on the effect of the relativistic phase space factor from Ref. [8] on the inclusive cross sections. With $\omega \equiv E - \sqrt{M_l^2 + \mathbf{k}'^2} \equiv E - E'$ and $\mathbf{Q} \equiv \mathbf{k} - \mathbf{k}'$ we write

$$\frac{d\sigma}{d^3\mathbf{k}'} \sim \delta\left(\omega + M_d - \sqrt{M_p^2 + \mathbf{p}_1^2} - \sqrt{M_p^2 + \mathbf{p}_2^2}\right) \delta^3(\mathbf{Q} - \mathbf{p}_1 - \mathbf{p}_2) d^3\mathbf{p}_1 d^3\mathbf{p}_2. \quad (2.19)$$

By changing variables from the individual nucleons' momenta (\mathbf{p}_1 and \mathbf{p}_2) to the total (\mathbf{p}_{12}) and relative one (\mathbf{p}), we rewrite (2.19) as

$$\frac{d\sigma}{d^3\mathbf{k}'} \sim \delta\left(\omega + M_d - \sqrt{M_p^2 + \left(\mathbf{p} + \frac{1}{2}\mathbf{Q}\right)^2} - \sqrt{M_p^2 + \left(\mathbf{p} - \frac{1}{2}\mathbf{Q}\right)^2}\right) d^3\mathbf{p}. \quad (2.20)$$

Defining $x \equiv \hat{\mathbf{p}} \cdot \hat{\mathbf{Q}}$ and $Q \equiv |\mathbf{Q}|$ we evaluate (2.20) as

$$\frac{d\sigma}{d^3\mathbf{k}'} \sim \int_{-1}^1 dx \frac{p^2}{\left| \frac{p+Qx/2}{E_1} + \frac{p-Qx/2}{E_2} \right|}, \quad (2.21)$$

where $E_{1,2} \equiv \sqrt{M_p^2 + (p \pm Qx/2)^2}$ and $p = \frac{(M_d+\omega) \sqrt{-4M_p^2+(M_d+\omega-Q)(M_d+\omega+Q)}}{2 \sqrt{(M_d+\omega-Qx)(M_d+\omega+Qx)}}$.

The corresponding nonrelativistic evaluation starts with

$$\frac{d\sigma}{d^3\mathbf{k}'} \sim \delta \left(\omega + M_d - 2M_p - \frac{\mathbf{p}_1^2}{2M_p} - \frac{\mathbf{p}_2^2}{2M_p} \right) \delta^3(\mathbf{Q} - \mathbf{p}_1 - \mathbf{p}_2) d^3\mathbf{p}_1 d^3\mathbf{p}_2 \quad (2.22)$$

and the same change of variables yields after standard steps

$$\frac{d\sigma}{d^3\mathbf{k}'} \sim \int_{-1}^1 dx \frac{1}{2} M_p p_{nrl}, \quad (2.23)$$

where $p_{nrl} = \sqrt{M_p \left(\omega + M_d - 2M_p - \frac{\mathbf{Q}^2}{4M_p} \right)}$.

In Fig. 2 we compare the relativistic, $\rho_{rel} = \frac{p^2}{\left| \frac{p+Qx/2}{E_1} + \frac{p-Qx/2}{E_2} \right|}$, and the nonrelativistic, $\rho_{nrl} = \frac{1}{2} M_p p_{nrl}$, phase space factors. For a fixed initial electron neutrino energy and just one lepton scattering angle $\theta = \pi/2$ we calculate the phase space factors as a function of the outgoing lepton momentum k' . The relativistic phase space factor depends not only on the magnitude of the relative momentum p but also on x , so we calculate ρ_{rel} for seven x values: $-1, -2/3, -1/3, 0, 1/3, 2/3$ and 1 to check how strong the dependence on x is. For $E=50$ MeV all upper curves representing relativistic results with different x values essentially overlap, but for $E=300$ MeV the spread due to the different x values is clearly visible. The relativistic phase space factors are larger in the whole range of the k' momentum. The difference is particularly strong for small k' values and for $E=300$ MeV it exceeds 20 %. For $E=50$ MeV it is much smaller and reaches about 3 %.

B. The 2N scattering states in coordinate and momentum spaces

The nuclear matrix element, $\langle \Psi_f \mathbf{P}_f m_f | j_{CC}^\lambda | \Psi_i \mathbf{P}_i m_i \rangle$, involves the initial deuteron state and the 2N scattering state,

$$\begin{aligned} \langle \Psi_f \mathbf{P}_f m_f | j_{CC}^\lambda | \Psi_i \mathbf{P}_i m_i \rangle &= \langle \mathbf{p} \mathbf{P}_f = \mathbf{k} - \mathbf{k}' m_1 m_2 | j_{CC}^\lambda | \phi_d \mathbf{P}_i = 0 m_d \rangle \\ &= \langle \mathbf{p} \mathbf{P}_f = \mathbf{k} - \mathbf{k}' m_1 m_2 | \left(1 + t(E_{2N}) G_0^{2N}(E_{2N}) \right) j_{CC}^\lambda | \phi_d \mathbf{P}_i = 0 m_d \rangle \\ &= \langle \mathbf{p} m_1 m_2 | \left(1 + t(E_{2N}) G_0^{2N}(E_{2N}) \right) j_{CC}^\lambda(\mathbf{P}_f, \mathbf{P}_i) | \phi_d m_d \rangle \equiv N^\lambda \end{aligned} \quad (2.24)$$

obtained, for a given NN potential V , from the t matrix - solution of the Lippmann-Schwinger equation:

$$t(E_{2N}) = V + t(E_{2N}) G_0^{2N}(E_{2N}) V, \quad (2.25)$$

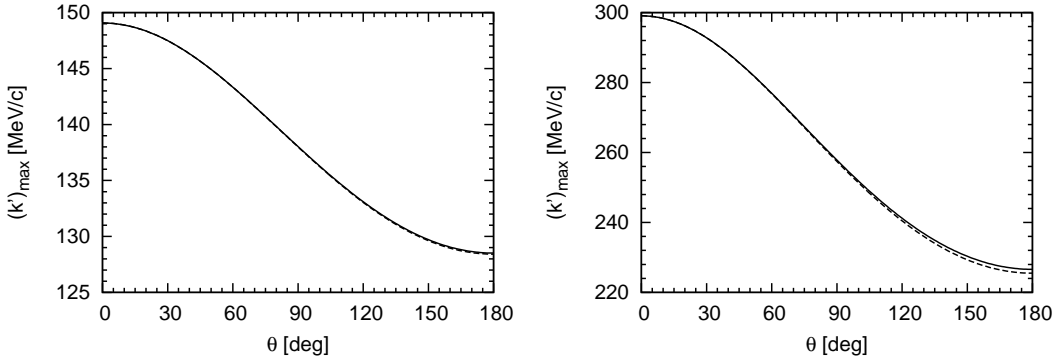


FIG. 1. Maximal value of the outgoing electron momentum k' in the $\nu_e + {}^2\text{H} \rightarrow e^- + p + p$ reaction as a function of the lepton scattering angle θ in the laboratory frame, calculated relativistically (solid line) and nonrelativistically (dashed line) for the incoming neutrino energy $E = 150$ MeV (left panel) and $E = 300$ MeV (right panel).

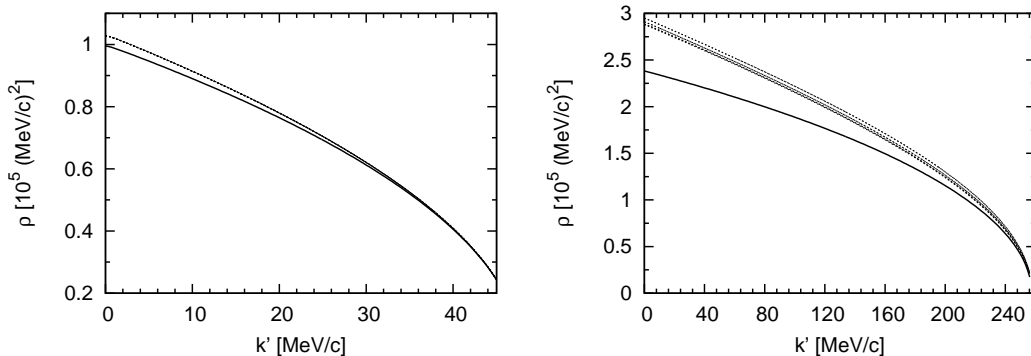


FIG. 2. The relativistic (group of dotted lines) and nonrelativistic (solid line) phase space factors compared for the initial neutrino energy $E = 50$ MeV (left panel) and $E = 300$ MeV (right panel) for the lepton scattering angle $\theta = \pi/2$ as a function of the outgoing lepton momentum k' . The group of dotted curves represent results with different values of x (see text). Note that these different predictions overlap for $E = 50$ MeV.

where $G_0^{2N}(E_{2N})$ is the free 2N propagator and the kinetic energy of the relative motion in the 2N system in our nonrelativistic approximation, $E_{2N} = \frac{\mathbf{p}^2}{M}$, is given by Eq. (2.13).

As already stated, we generate the deuteron wave function and solve Eq. (2.25) in momentum space, using the 2N partial wave states, $|p(ls)jm_j; tm_t\rangle$. They carry information about the magnitude of the relative momentum (p), the relative angular momentum (l), spin (s) and total angular momentum (j) with its corresponding projection (m_j). This set of quantum numbers is supplemented by the 2N isospin (t) and its projection (m_t). In the present work we employ all partial wave states with $j \leq 4$. Such calculations, closely corresponding to the ones presented in Ref. [62], are fully sufficient for the antineutrino induced CC reactions and the NC driven reactions, where only short-range potentials act between the two outgoing nucleons.

The neutrino induced CC reactions lead, however, in the final state to two protons, which interact also by the long-range Coulomb potential. The 2N scattering problem involving

this interaction is usually solved in coordinate space. We could follow the steps outlined in Ref. [8], but we wanted to take advantage of momentum space framework developed for the muon capture reaction. That is why we decided to perform standard momentum space t matrix calculations for the short-range potential. Thus the proton-proton version of the AV18 potential was supplemented by the sharply cut off Coulomb force V_{RC} , whose matrix elements are given by the following integral

$$\langle p'(l's')j'm_{j'}; t'm_{t'} | V_{RC} | p(ls)jm_j; tm_t \rangle = \delta_{l'l'} \delta_{s's'} \delta_{j'j} \delta_{m_j m_{j'}} \delta_{t't'} \delta_{m_t m_{t'}} \delta_{t_1} \delta_{m_{t_1}} 8\alpha \int_0^{R_C} dr r j_l(p'r) j_l(pr), \quad (2.26)$$

where $j_l(pr)$ is the spherical Bessel function and α is the fine structure constant. The value of the sharp cut-off was taken to be $R_C=40$ fm. This approach is fully justified by the observation that the current matrix elements Bessel transformed to coordinate space,

$$\langle r(ls)jm_j | j_{CC}^\lambda | \phi_d m_d \rangle = \frac{2}{\pi} i^l \int_0^\infty dk k^2 j_l(kr) \langle k(ls)jm_j | j_{CC}^\lambda | \phi_d m_d \rangle, \quad (2.27)$$

become negligible for $r \geq 30$ fm. This is illustrated in Fig. 3 for one (essentially arbitrary) lepton kinematics and few choices of discrete quantum numbers.

Additionally we checked that our momentum space generated 2N scattering states are fully equivalent to the radial wave functions calculated directly in coordinate space, using the collocation method from Refs. [73–75]. To this end we employed the well-known formula (see for example [8] and references therein), which using our normalization of states, reads

$$\psi_{l'sls}^j(r) = \delta_{l'l} j_l(pr) + i^{l-l'} M \int_0^\infty \frac{dk k^2 j_{l'}(kr)}{p^2 - k^2 + i\epsilon} \langle k(l's)j | t(E_{2N}) | p(ls)j \rangle. \quad (2.28)$$

This is exemplified in Figs.4–7, for two E_{2N} energies (5 and 50 MeV) and two partial wave cases (1S_0 and $^3P_2 - ^3F_2$). In all cases we get a perfect agreement in the whole range of r values, from $r=0$ to $r=40$ fm.

C. The cross section

Having discussed all the elements of our formalism, we can give the main formula for the cross section, consistent with the momentum space formalism presented in the previous subsections. We do it for the $\nu_e + ^2\text{H} \rightarrow e^- + p + p$ reaction and discuss later some differences if other reactions are considered. With our normalization of the N^λ matrix elements we start with [72]

$$d\sigma = \frac{1}{|\mathbf{v}_1 - \mathbf{v}_2|} \frac{1}{2E} (L_\alpha)^* L_\beta (N^\alpha)^* N^\beta \frac{G_F^2 \cos^2 \theta_C}{2} \times F(Z, k') \frac{d^3 \mathbf{k}'}{2E'} \frac{d^3 \mathbf{p}_1}{(2\pi)^3} \frac{d^3 \mathbf{p}_2}{(2\pi)^3} (2\pi)^4 \delta^4(P' - P) \mathcal{S}, \quad (2.29)$$

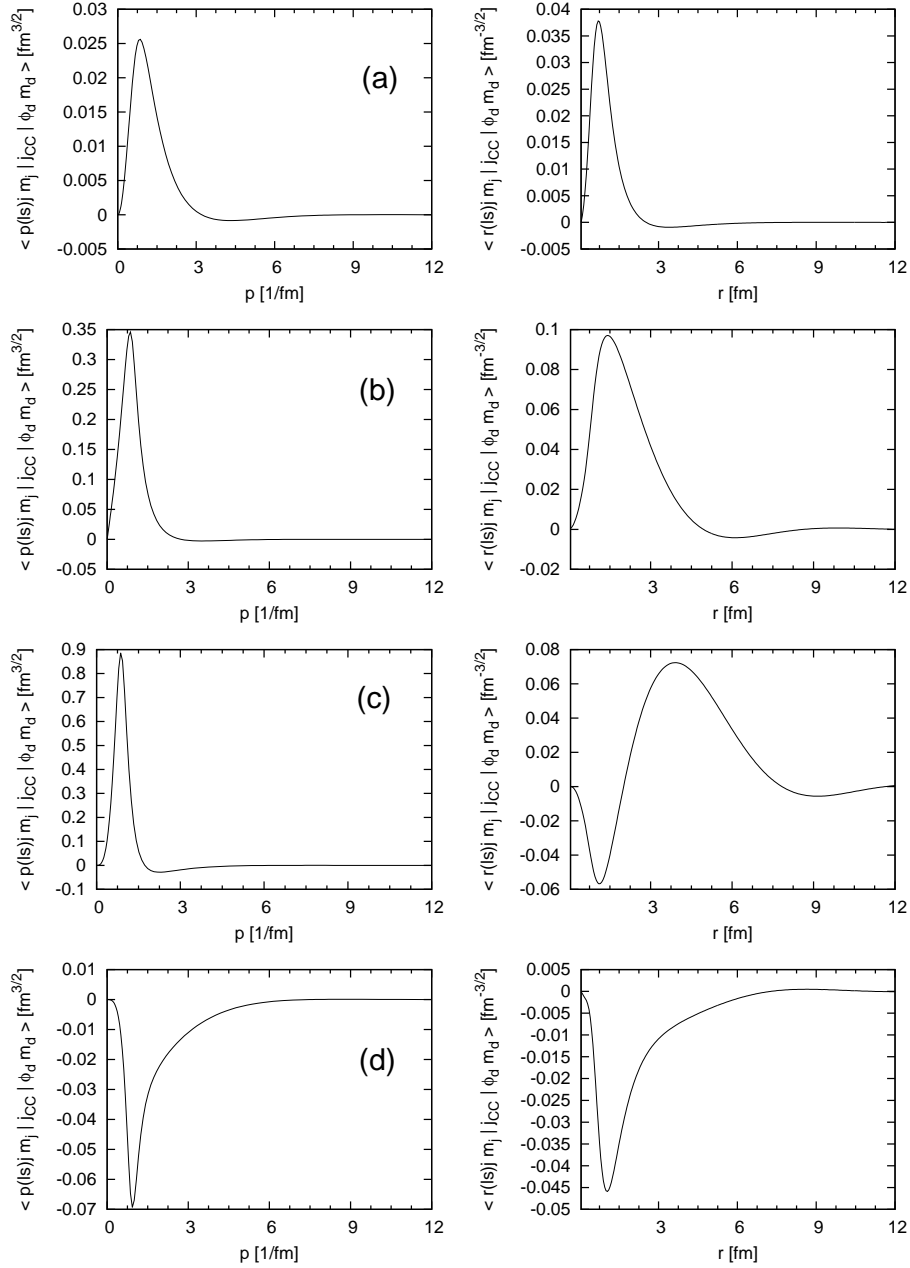


FIG. 3. Matrix elements of the single nucleon weak CC operator in the partial wave basis of momentum space (left panel) and of coordinate space (right panel) for one selected lepton kinematics of the $\bar{\nu}_e + {}^2\text{H} \rightarrow e^+ + n + n$ reaction: $E = 300$ MeV, $\theta = 100^\circ$, $E' = 172$ MeV ($\omega = 128$ MeV, $Q = 354$ MeV, $E_{2N} = 91$ MeV). The rows correspond to the different choices of the projection of the total deuteron spin m_d , the component of the current operator j_{CC}^λ and the final 2N channel. From top to bottom: ((a) $m_d = 0, j_{CC}^0, {}^1S_0$), ((b) $m_d = -1, j_{CC+1}, {}^3P_2$), ((c) $m_d = +1, j_{CC-1}, {}^3F_2$), ((d) $m_d = 0, j_{CCz}, {}^3F_2$). Note that the factor i^l is skipped in the Bessel transform.

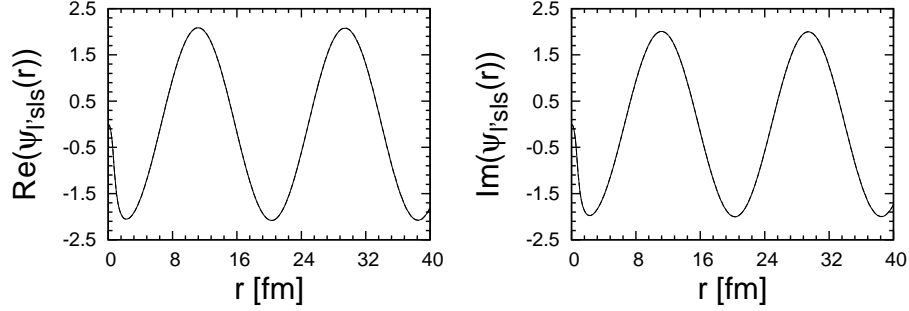


FIG. 4. The scattering radial wave function $\psi_{l'sls}(r)$ obtained directly in coordinate space (solid line) compared to the one generated from the solution of the Lippmann-Schwinger equation obtained in momentum space (dashed line) for the internal $2N$ energy $E_{2N} = 5$ MeV for the uncoupled 1S_0 channel. The wave functions are calculated with the strong proton-proton potential augmented by a sharply cut off Coulomb potential with the cut-off value $R_C = 40$ fm. The real (imaginary) parts of the wave functions are displayed in the left (right) panel. The solid and dashed lines fully overlap.

where in the laboratory frame the relative velocity of the projectile and target $|\mathbf{v}_1 - \mathbf{v}_2|$ is equal $c (= 1)$ and the \mathcal{S} factor is needed when in the final state identical particles appear. The Fermi function $F(Z, k')$ [76] is introduced to account for the Coulomb modification of the final lepton wave functions by the two protons in the final state and is not needed otherwise. (Note that in L_α we use the following normalization for the Dirac spinors: $\bar{u}u = 2M_l$ and $\bar{v}v = -2M_l$.) Defining

$$\widetilde{L}_{\alpha\beta} = \sum_{m_\nu} \sum_{m_{l^-}} (L_\alpha)^* L_\beta, \quad (2.30)$$

taking all factors into account and evaluating the phase space factor in terms of the relative momentum, we arrive at the following expression for the total cross section

$$\begin{aligned} \sigma_{tot} = & \frac{G_F^2 \cos^2 \theta_C}{2(2\pi)^2} \frac{1}{4E} \int_0^{2\pi} d\phi \int_0^\pi d\theta \sin \theta \int_{M_l}^{E'_{max}} dE' k' \frac{1}{2} M_p p_{nrl} \\ & \times F(Z, k') \int_0^{2\pi} d\phi_p \int_0^\pi d\theta_p \sin \theta_p \frac{2}{3} \sum_{m_1, m_2} \sum_{m_d} \widetilde{L}_{\alpha\beta} (N^\alpha)^* N^\beta, \end{aligned} \quad (2.31)$$

where the θ and ϕ angles describe the direction of the outgoing lepton in the laboratory frame. Note that for the total unpolarized cross section considered here the integral over the azimuthal angle ϕ can be replaced by the factor 2π .

The contraction $|T|^2 \equiv \widetilde{L}_{\alpha\beta} (N^\alpha)^* N^\beta$ can be written in terms of the V_{ij} functions stemming from the lepton arm and the products of the nuclear matrix elements N^α . For the latter we use the spherical components and obtain

$$\begin{aligned} |T|^2 = & V_{00} |N^0|^2 + V_{MM} |N_{-1}|^2 + V_{PP} |N_{+1}|^2 \\ & + V_{ZZ} |N_z|^2 + V_{Z0} N_z (N^0)^* + V_{0Z} N^0 (N_z)^*, \end{aligned} \quad (2.32)$$

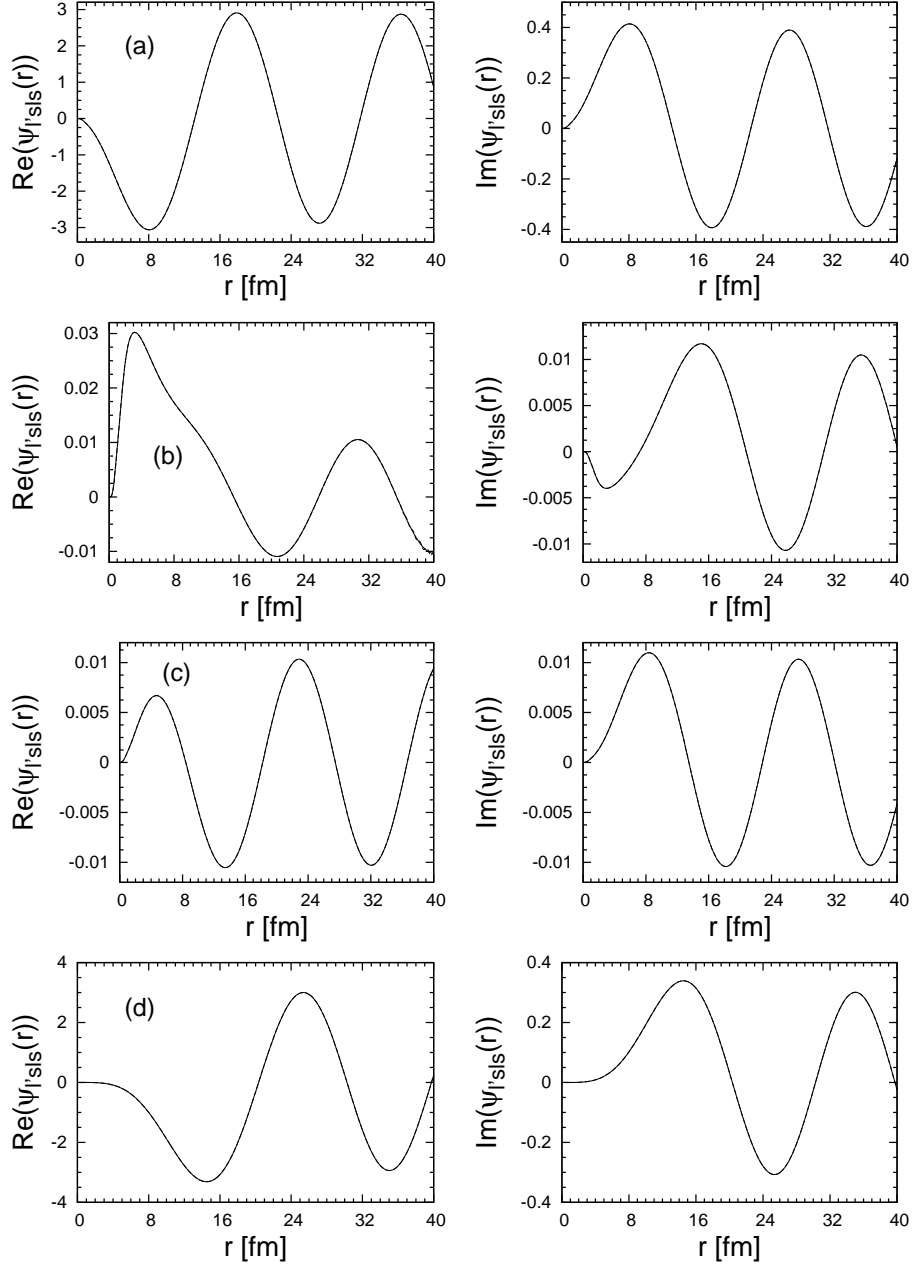


FIG. 5. The same as in Fig. 4 but for the coupled ${}^3P_2 - {}^3F_2$ channels. The real (imaginary) parts of the wave functions are displayed in the left (right) panels and the rows from top to bottom correspond to different $l'l$ pairs: ((a) ${}^3P_2 - {}^3P_2$), ((b) ${}^3F_2 - {}^3P_2$), ((c) ${}^3P_2 - {}^3F_2$) and ((d) ${}^3F_2 - {}^3F_2$).

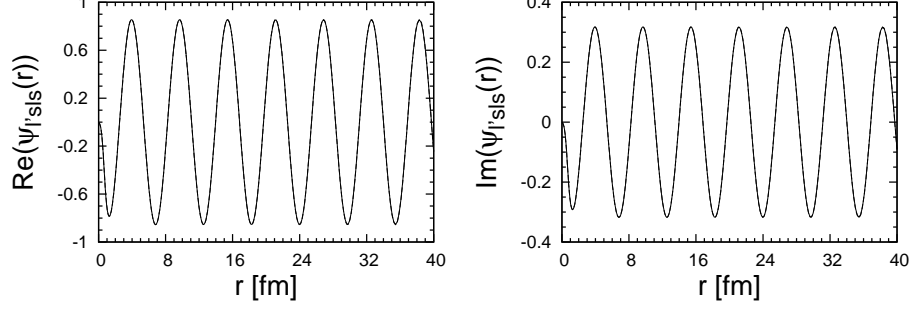


FIG. 6. The same as in Fig. 4 but for the internal 2N energy $E_{2N} = 50$ MeV.

where for the neutrino induced reactions

$$\begin{aligned}
V_{00} &= 8 (\mathbf{k}' \cdot \mathbf{k} + E E') , \\
V_{MM} &= 8 (E + k_z) (E' - k'_z) , \\
V_{PP} &= 8 (E - k_z) (E' + k'_z) , \\
V_{ZZ} &= 8 (-\mathbf{k}' \cdot \mathbf{k} + E E') , \\
V_{Z0} &= -8 (E k'_z + E' k_z) + 8i (k'_y k_x - k'_x k_y) , \\
V_{0Z} &= -8 (E k'_z + E' k_z) + 8i (k'_x k_y - k'_y k_x) .
\end{aligned} \tag{2.33}$$

The corresponding \bar{V}_{ij} functions for the antineutrino induced reactions are given as:

$$\begin{aligned}
\bar{V}_{00} &= V_{00} , \\
\bar{V}_{MM} &= V_{PP} , \\
\bar{V}_{PP} &= V_{MM} , \\
\bar{V}_{ZZ} &= V_{ZZ} , \\
\bar{V}_{Z0} &= V_{0Z} , \\
\bar{V}_{0Z} &= V_{Z0} .
\end{aligned} \tag{2.34}$$

In the following we assume the system of coordinates, where $\mathbf{Q} \equiv \mathbf{k} - \mathbf{k}' \parallel \hat{z}$ and $\hat{y} = \frac{\mathbf{k} \times \mathbf{k}'}{|\mathbf{k} \times \mathbf{k}'|}$, so

$$\begin{aligned}
k'_x &= k_x = |\mathbf{k}| |\mathbf{k}'| \sin \theta / |\mathbf{Q}| , \\
k'_y &= k_y = 0 , \\
k_z &= |\mathbf{k}| (|\mathbf{k}| - |\mathbf{k}'| \cos \theta) / |\mathbf{Q}| , \\
k'_z &= |\mathbf{k}'| (-|\mathbf{k}'| + |\mathbf{k}| \cos \theta) / |\mathbf{Q}| , \\
|\mathbf{Q}| &= \sqrt{\mathbf{k}^2 + \mathbf{k}'^2 - 2 |\mathbf{k}| |\mathbf{k}'| \cos \theta} .
\end{aligned} \tag{2.35}$$

As a consequence, we get further simplifications:

$$\bar{V}_{0Z} = \bar{V}_{Z0} = V_{0Z} = V_{Z0} . \tag{2.36}$$

The main reason to use the spherical components of the current operator and the system of coordinates defined above is that we get in this case the simplest relations between the total

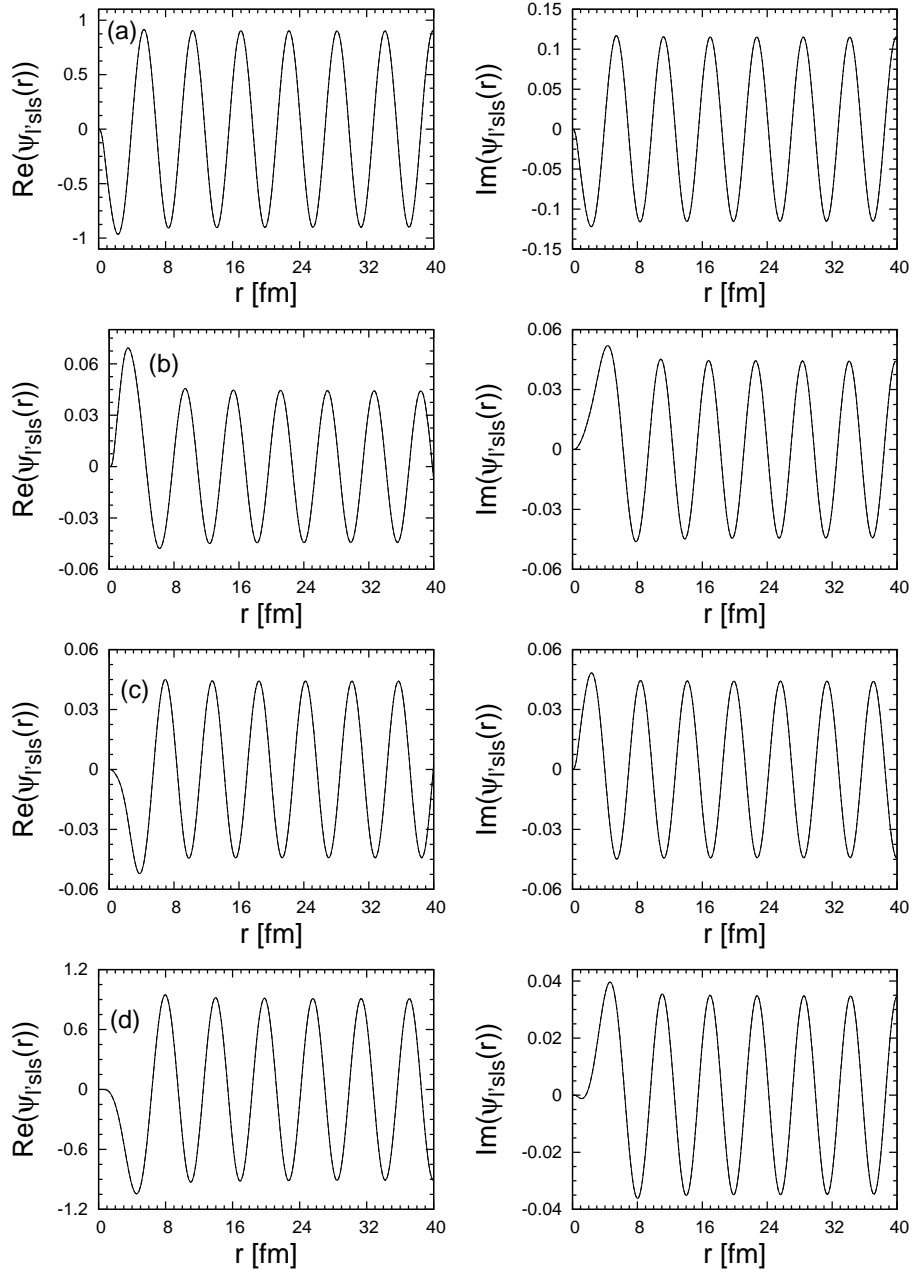


FIG. 7. The same as in Fig. 5 but for the internal 2N energy $E_{2N} = 50$ MeV.

spin magnetic quantum numbers m_d and m_j for matrix elements $\langle p(ls)jm_j | j_{CC}^\lambda | \phi_d m_d \rangle$ in the partial wave representation:

$$\begin{aligned}
 \langle p(ls)jm_j | j_{CC}^0 | \phi_d m_d \rangle &\propto \delta_{m_j, m_d}, \\
 \langle p(ls)jm_j | j_{CC,z} | \phi_d m_d \rangle &\propto \delta_{m_j, m_d}, \\
 \langle p(ls)jm_j | j_{CC,\pm 1} | \phi_d m_d \rangle &\propto \delta_{m_j \pm 1, m_d}.
 \end{aligned}
 \tag{2.37}$$

For the neutral current (NC) driven processes Eq. (2.31) has to be modified. The Fermi function $F(Z, k')$ and $\cos^2 \theta_C$ are replaced by 1, but most importantly the weak CC operator j_{CC}^λ is replaced by the corresponding NC operator j_{NC}^λ . Its construction is described in detail

in Refs. [2, 8] and we follow Ref. [8] for the choice of the nucleon form factors. Since we employ only the single nucleon current, we use the given prescription for the proton and neutron NC operators and, using the isospin formalism, define the current of nucleon i as

$$j_{NC}(i) = \frac{1}{2}(1 + \tau_3(i))j_{NC}^p + \frac{1}{2}(1 - \tau_3(i))j_{NC}^n \quad (2.38)$$

in full analogy to the electromagnetic single nucleon current. Of course, also in this case the relations (2.38) remain true.

D. The 3N matrix elements

We treat the ${}^3\text{He}$ (${}^3\text{H}$) disintegration process analogously to the 2N reactions. The 3N Hamiltonian H comprises the 3N kinetic energy (H_0), two-body subsystem potential energies (V_{12} , V_{23} and V_{31}) as well as the three-body potential energy (V_{123}). The latter quantity is usually called a 3N force (3NF) and is decomposed into three terms

$$V_{123} = V^{(1)} + V^{(2)} + V^{(3)}, \quad (2.39)$$

where $V^{(i)}$ is symmetric under exchange of nucleons j and k ($i, j, k = 1, 2, 3, i \neq j \neq k \neq i$). The 3N bound state wave function is calculated using the method described in Ref. [77]. The Faddeev equation for the Faddeev component $|\psi\rangle$ reads

$$|\psi\rangle = G_0 t_{23} P |\psi\rangle + (1 + G_0 t_{23}) G_0 V^{(1)} (1 + P) |\psi\rangle. \quad (2.40)$$

Here $G_0 \equiv 1/(E - H_0)$ is the free 3N propagator and $P \equiv P_{12}P_{23} + P_{13}P_{23}$ is the permutation operator built from transpositions P_{ij} , which interchange nucleons i and j . Note that the two-body t -operator t_{23} acts now in the 3N space. The full wave function $|\Psi\rangle$ is easily obtained from the Faddeev component as

$$|\Psi\rangle = (1 + P) |\psi\rangle. \quad (2.41)$$

The 3N current operator j_{3N}^μ contains the single-nucleon, 2N and, in principle, also the 3N contribution. Therefore we write:

$$j_{3N}^\mu = j_1^\mu + j_2^\mu + j_3^\mu + j_{12}^\mu + j_{23}^\mu + j_{31}^\mu + j_{123}^\mu, \quad (2.42)$$

where the 3N part can be split into three components (just like the 3NF), $j_{123}^\mu = j^{\mu 1} + j^{\mu 2} + j^{\mu 3}$. Thus we can decompose the 3N current operator into three parts, $j^\mu(i)$ ($i = 1, 2, 3$), which possess the same symmetry properties as $V^{(i)}$:

$$j_{3N}^\mu = j^\mu(1) + j^\mu(2) + j^\mu(3), \quad (2.43)$$

where for example $j^\mu(1) \equiv j_1^\mu + j_{23}^\mu + j^{\mu 1}$.

With all these ingredients, we construct the matrix elements for the nucleon-deuteron (Nd)

$$N_{Nd}^\mu = \langle \Psi_{Nd}^{(-)} | j_{3N}^\mu | \Psi \rangle \quad (2.44)$$

and the 3N break-up channel

$$N_{3N}^\mu = \langle \Psi_{3N}^{(-)} | j_{3N}^\mu | \Psi \rangle, \quad (2.45)$$

with the corresponding channel scattering states. To this end first we solve a Faddeev-type equation for an auxiliary state $|U^\mu\rangle$ [79],

$$\begin{aligned} |U^\mu\rangle = & \left(t_{23}G_0 + \frac{1}{2}(1+P)V^{(1)}G_0(1+t_{23}G_0) \right) (1+P)j^\mu(1)|\Psi\rangle \\ & + \left(t_{23}G_0P + \frac{1}{2}(1+P)V^{(1)}G_0(1+t_{23}G_0)P \right) |U^\mu\rangle, \end{aligned} \quad (2.46)$$

which depends on the component of the current operator and two kinematical quantities, but is independent of the final state kinematics. The two kinematical quantities are the 3N internal energy $E_{c.m.}$ and the magnitude of the three-momentum transferred to the 3N system, $|\mathbf{Q}|$. In practice we use the density operator $\rho \equiv j_{3N}^0$ as well as the spherical components of the current operator

$$\begin{aligned} j_{+1} &\equiv -\frac{1}{\sqrt{2}}(j_{3N}^1 + ij_{3N}^2) \equiv -\frac{1}{\sqrt{2}}(j_{x3N} + ij_{y3N}), \\ j_{-1} &\equiv \frac{1}{\sqrt{2}}(j_{3N}^1 - ij_{3N}^2) \equiv \frac{1}{\sqrt{2}}(j_{x3N} - ij_{y3N}) \end{aligned} \quad (2.47)$$

and choose \mathbf{Q} parallel to the z -axis. As in the 2N case, this yields the simplest relations between the total 3N angular momentum projections of the initial and final nuclear systems.

The matrix elements N_{Nd}^μ and N_{3N}^μ for arbitrary exclusive kinematics are then obtained by simple quadratures:

$$N_{Nd}^\mu = \langle\phi_{Nd} | (1+P)j^\mu(1) | \Psi\rangle + \langle\phi_{Nd} | P | U^\mu\rangle, \quad (2.48)$$

$$\begin{aligned} N_{3N}^\mu = & \langle\phi_{3N} | (1+P)j^\mu(1) | \Psi\rangle + \langle\phi_{3N} | t_{23}G_0(1+P)j^\mu(1) | \Psi\rangle \\ & + \langle\phi_{3N} | P | U^\mu\rangle + \langle\phi_{3N} | t_{23}G_0P | U^\mu\rangle, \end{aligned} \quad (2.49)$$

where $|\phi_{Nd}\rangle$ is a product of the internal deuteron state and the state describing the free relative motion of the third nucleon with respect to the deuteron and $|\phi_{3N}\rangle$ is a state (antisymmetrized in the (2,3) subsystem) representing the free motion of the three outgoing nucleons. Exclusive observables can be further integrated over suitable phase space domains to arrive at the semi-exclusive or inclusive observables.

Inclusive observables can be, however, also computed in a different way, without any resort to explicit final state kinematics [78, 79]. In inclusive calculations, where only the final energy E of the nuclear system is known, one encounters the so-called "response functions", which are defined through the following integral

$$R_{AB}^{inc} = \sum_{m_i, m_f} \int df \delta(E - E_f) \langle\Psi_f^{(-)} | j_{3N}^A | \Psi\rangle \left(\langle\Psi_f^{(-)} | j_{3N}^B | \Psi\rangle \right)^*, \quad (2.50)$$

and depend, in general, on two components of the nuclear current operator, A and B . In Eq. (2.50) m_i and m_f represent the whole sets of the initial and final spin magnetic quantum numbers, respectively, while the df integral denotes the sum and the integration over all final 3N states with the energy E . Using closure, Eq. (2.50) can be rewritten as

$$R_{AB}^{inc} = \sum_{m_i} \int df \langle\Psi | (j_{3N}^B)^\dagger \delta(E - H) j_{3N}^A | \Psi\rangle, \quad (2.51)$$

where H is again the full 3N Hamiltonian and the 3N bound state does not contribute to the df integration for $E > 0$. Within the Faddeev scheme [78, 79], R_{AB}^{inc} can be expressed in terms of some auxiliary states as

$$\begin{aligned} R_{AB}^{inc} &= \frac{1}{2\pi i} \sum_{m_i} \left(\langle \Psi | (j_{3N}^A)^\dagger | \Psi^B \rangle^* - \langle \Psi | (j_{3N}^B)^\dagger | \Psi^A \rangle \right) \\ &= \frac{3}{2\pi i} \sum_{m_i} \left(\langle \Psi | (j^A(1))^\dagger G_0(1+P) | V^B \rangle^* - \langle \Psi | (j^B(1))^\dagger G_0(1+P) | V^A \rangle \right), \end{aligned} \quad (2.52)$$

where in turn ($C = A, B$)

$$| \Psi^C \rangle = G_0(1+P) | V^C \rangle. \quad (2.53)$$

The state $| V^C \rangle$ obeys the Faddeev-type equation

$$\begin{aligned} | V^C \rangle &= (1 + t_{23}G_0) j^C(1) | \Psi \rangle \\ &+ \left(tG_0P + (1 + t_{23}G_0) V^{(1)}G_0 (1 + P) \right) | V^C \rangle, \end{aligned} \quad (2.54)$$

with the same integral kernel as in the treatment of 3N scattering [80]. Interestingly, the relation between the auxiliary states defined in Eqs. (2.46) and (2.54) is very simple when the 3N force is neglected:

$$| V^C \rangle = j^C(1) | \Psi \rangle + | U^C \rangle. \quad (2.55)$$

The fact that R_{AB}^{inc} can be obtained by direct integrations or employing the method described above is used by us to test the numerical performance.

All the 3N Faddeev-type equations are solved by iterations in the momentum-space basis

$$| p q \alpha \rangle \equiv | p q (ls) j \left(\lambda \frac{1}{2} \right) I(jI) J m_J \left(t \frac{1}{2} \right) T m_T \rangle, \quad (2.56)$$

which is an extension of the (2,3) subsystem basis $| p \alpha_2 \rangle$. Here q is the magnitude of the Jacobi momentum, which describes the motion of the spectator nucleon 1 with respect to the center of mass of the (2,3) subsystem. Consequently, the orbital angular momentum λ of the spectator nucleon and its spin $\frac{1}{2}$ couple to the total spectator angular momentum I . The total angular momentum of the subsystem (j) and the total angular momentum of nucleon 1 (I) couple eventually to the total angular momentum of the 3N system J and its projection m_J . A corresponding coupling is introduced in the isospin space, where the (2,3) total subsystem isospin (t) together with the isospin of nucleon 1 builds the total 3N isospin T with the projection m_T . In practise, the calculations are restricted to a finite set of $| p \alpha_2 \rangle$ and $| p \alpha \rangle$ states, which fulfill the condition $j \leq j_{max}$ and $J \leq J_{max}$. For the studied here low 3N internal energies and momentum transfers convergence is achieved already with $j_{max} = 3$ and $J_{max} = \frac{15}{2}$.

In the following sections we describe our results, which are obtained, like in Ref. [8], without considering radiative corrections. Information about possible modifications of the results due to these effects are discussed in Ref. [51] and references cited therein.

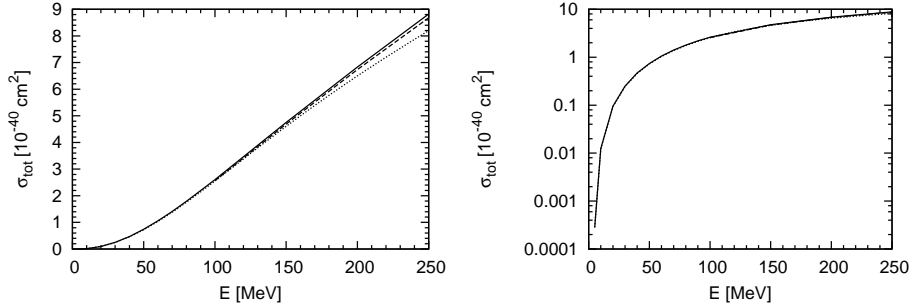


FIG. 8. The total cross section for the $\bar{\nu}_e + {}^2\text{H} \rightarrow e^+ + n + n$ reaction as a function of the initial antineutrino energy E shown on a linear (left panel) and on a logarithmic (right panel) scale. The dashed (solid) line shows coordinate space predictions from Tabs. II and IV of Ref. [8] obtained with the AV18 potential and with the single nucleon current (with the inclusion of single- and 2N terms in the weak current operator), employing the relativistic kinematics. The dotted line displays results of nonrelativistic momentum space calculations from the present work obtained with the AV18 potential and with the single nucleon current.

III. RESULTS FOR NEUTRINO SCATTERING ON ${}^2\text{H}$

Although on the way to calculate the total cross sections we evaluate the necessary integrands - the differential cross sections - we show here only the inclusive observables. Whenever it is possible, we compare our momentum-space results with the predictions from Shen *et al.* [8], which are also based on the traditional dynamical input. Since our calculations are strictly nonrelativistic, we restrict ourselves to the neutrino energies up to 250 MeV.

Let us start with the total cross section for the $\bar{\nu}_e + {}^2\text{H} \rightarrow e^+ + n + n$ reaction, as it is the closest to the muon capture process studied in Ref. [62]. It is shown in Fig. 8 as a function of the initial antineutrino energy E , both on a linear and on a logarithmic scale. The dashed and solid lines in this figure show the predictions from Tabs. II and IV of Ref. [8] obtained with the AV18 potential and with the single-nucleon current as well as with the single-nucleon current supplemented by the 2N currents linked to the AV18 potential. The difference between these two curves highlights the importance of the 2N currents for this reaction. The third, dotted, line is used to display results of our nonrelativistic calculations, carried out in momentum space with the AV18 potential and with the single nucleon current. Clearly for the energies $E \leq 100$ MeV all the three predictions essentially overlap, but for higher energies effects of 2N contributions to the current operator are visible. The relativistic treatment of the kinematics by Shen *et al.* leads to a clear spread between the dashed and the dotted line.

Next, in Fig. 9 we display in the same way results for the other CC driven reaction: $\nu_e + {}^2\text{H} \rightarrow e^- + p + p$. Again our nonrelativistic predictions from momentum-space calculations are compared with the results from Ref. [8]. The values of the cross section are several times bigger and they rise with the neutrino energy at a different pace than for the antineutrino induced reaction. While the scale of the relativistic effects in the kinematics is the same, the 2N currents seem to play a more important role for the highest energies considered here.

Elastic NC driven (anti)neutrino scattering on ${}^2\text{H}$ has not been considered in Refs. [8, 51]. It was studied, for example by Frederico *et al.* [81] and later by Butler *et al.* [82], who

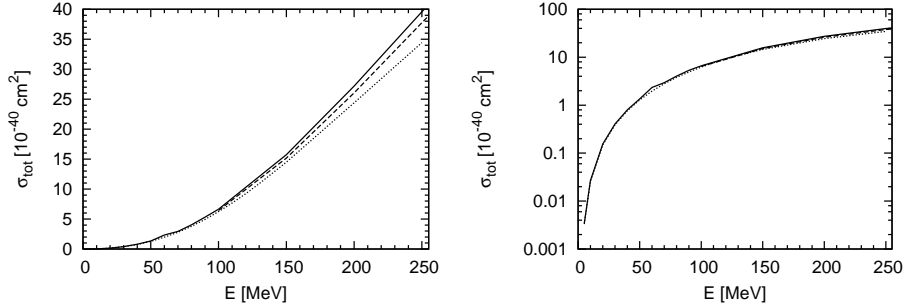


FIG. 9. The same as in Fig. 8 for the $\nu_e + {}^2\text{H} \rightarrow e^- + p + p$ reaction.

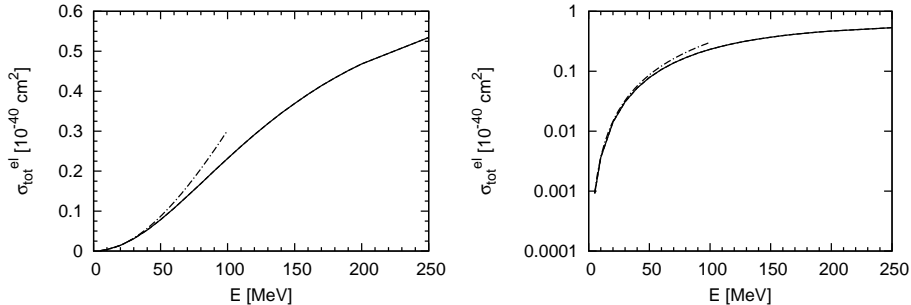


FIG. 10. The total cross section for the elastic NC (anti)neutrino scattering off the deuteron as a function of the initial (anti)neutrino energy E , shown on a linear (left panel) and on a logarithmic (right panel) scale. The solid line displays results of nonrelativistic momentum space calculations from the present work obtained with the AV18 potential and with the single nucleon current. These results are flavor independent and are the same for neutrino and antineutrino scattering. In addition the dash-dotted line corresponds to the results from Butler *et al.* [82], ignoring the strangeness contents of the deuteron. See text for more details.

investigated also the neutrino-deuteron break-up reactions within a χEFT approach at next-to-leading order (NLO). The authors of Ref. [82] derived analytical expressions for the elastic (anti)neutrino-deuteron scattering cross section, but did not yield direct results for the total cross sections. They were interested in the effects caused by the presence of the strange quarks in the deuteron. If the strangeness in the deuteron is neglected, the results for the elastic channel are not only flavor independent but just the same for neutrino and antineutrino scattering. That is exactly the case for our calculations presented in Fig. 10. At the considered here low (anti)neutrino energies, this reaction is extremely hard to measure, due to the very small deuteron recoil energy. In addition, this reaction channel is strongly suppressed, as can be seen in Fig. 10, resulting in very small values of the total cross sections. In Fig. 10, beside our predictions, we show also the results derived from Eq. (34) in Ref. [82], setting the strange form factors to zero and calculating the F_C form factor using the simple lowest-order (LO) expression given by Eq. (31) in that reference. For low (anti)neutrino energies, where the LO formula is valid, both types of results nicely agree and clearly diverge in the higher-energy region.

The inelastic NC induced reactions with the deuteron have been considered in Ref. [8] and in Figs. 11 and 12 we again compare results based on coordinate-space and momentum-space approaches, for the antineutrino and neutrino scattering, respectively. As in Fig. 8

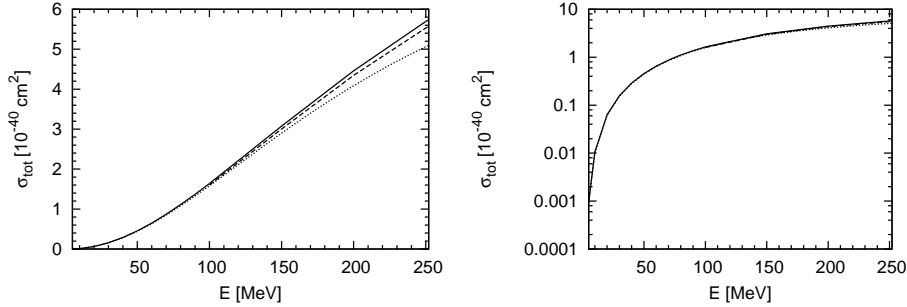


FIG. 11. The total cross section for the $\bar{\nu}_e + {}^2\text{H} \rightarrow \bar{\nu}_e + p + n$ reaction as a function of the initial antineutrino energy E shown on a linear (left panel) and on a logarithmic (right panel) scale. The dashed (solid) line shows coordinate space predictions from Tabs. II and III of Ref. [8] obtained with the AV18 potential and with the single nucleon current (with the inclusion of single- and 2N terms in the weak current operator), employing the relativistic kinematics. The dotted line displays results of nonrelativistic momentum space calculations from the present work obtained with the AV18 potential and with the single nucleon current.

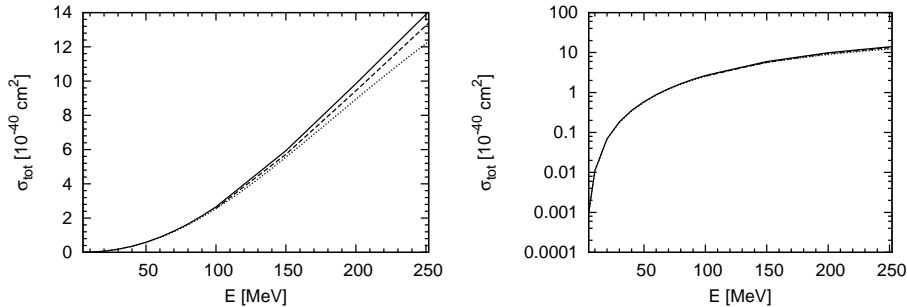


FIG. 12. The same as in Fig. 8 for the $\nu_e + {}^2\text{H} \rightarrow \nu_e + p + n$ reaction.

and 9, we use results of Ref. [8], now from Tabs. II and III, for the total cross section for the $\bar{\nu}_e + {}^2\text{H} \rightarrow \bar{\nu}_e + p + n$ and $\nu_e + {}^2\text{H} \rightarrow \nu_e + p + n$ reactions, respectively. The solid and dashed curves represent results from Ref. [8] with and without 2N contributions in the weak neutral nuclear current operator, accordingly. They have been calculated with the relativistic kinematics, so for higher energies in both figures the dashed lines visibly deviate from the dotted ones, representing our fully nonrelativistic momentum space predictions. These purely kinematical effects are of course essentially identical for the CC and NC driven reactions with electron (anti)neutrinos, as the electron mass is very small compared to higher beam energies, where to a good approximation the electron could be treated as massless. The cross sections for the NC neutrino induced reaction are bigger than for the corresponding reaction with the antineutrinos (roughly by a factor two), but this relative difference with respect to the antineutrino reaction is clearly smaller than for the CC induced reactions.

IV. RESULTS FOR NEUTRINO SCATTERING ON ${}^3\text{HE}$ AND ${}^3\text{H}$

The results presented in this section have also been obtained with the single nucleon weak current operator from Refs. [8, 48, 62] and with a nuclear Hamiltonian, which contains only

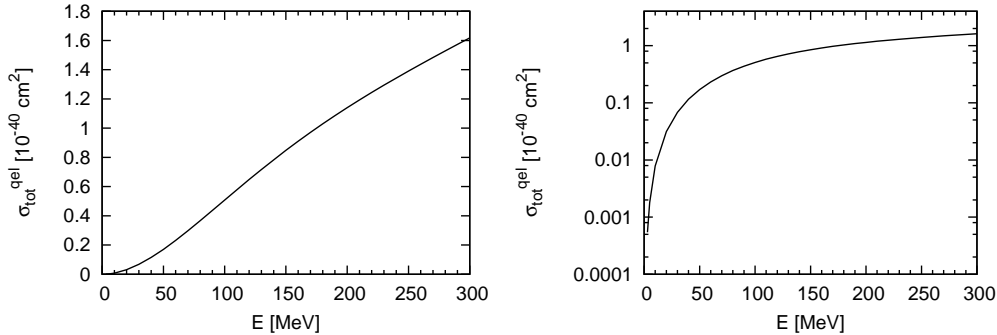


FIG. 13. The total cross section for the quasielastic CC $\bar{\nu}_e + {}^3\text{He} \rightarrow e^+ + {}^3\text{H}$ process as a function of the initial antineutrino energy E shown on the linear (left panel) and logarithmic (right panel) scale. The results are obtained with the AV18 NN potential and with the single nucleon CC operator, which contains the relativistic corrections.

the 2N potential energy - the 3N force has been neglected.

The same formalism which has been successfully developed for electron scattering and photodisintegration processes with 3N systems [78, 79] as well as for muon capture on the 3N bound states [62, 70] is directly applicable to elastic, quasi-elastic and inelastic (anti)neutrino scattering on ${}^3\text{He}$ and ${}^3\text{H}$. The key elements of this formalism are presented in Sec. II.

First we consider the quasi-elastic electron antineutrino scattering on ${}^3\text{He}$, leading to the positron and ${}^3\text{H}$ nucleus in the final state. In this process the same as in muon capture weak CC operator changes the total charge of the nuclear system. In Fig. 13 we show the total cross sections for the $\bar{\nu}_e + {}^3\text{He} \rightarrow e^+ + {}^3\text{H}$ reaction as a function of the initial antineutrino energy.

Further non-break-up reactions with trinucleons are possible only with the neutral current. In Fig. 14 we display the predictions for the total cross section of the elastic $\bar{\nu}_l + {}^3\text{He} \rightarrow \bar{\nu}_l + {}^3\text{He}$, $\bar{\nu}_l + {}^3\text{H} \rightarrow \bar{\nu}_l + {}^3\text{H}$, $\nu_l + {}^3\text{He} \rightarrow \nu_l + {}^3\text{He}$, and $\nu_l + {}^3\text{H} \rightarrow \nu_l + {}^3\text{H}$ reactions as a function of the initial (anti)neutrino energy. Despite very similar reaction kinematics, the cross sections take quite different values. The antineutrino- ${}^3\text{He}$ cross section is the smallest and the neutrino- ${}^3\text{H}$ cross section reaches the highest values. Lines representing neutrino- ${}^3\text{He}$ and antineutrino- ${}^3\text{H}$ cross sections cross at $E \approx 150$ MeV, with the former prevailing for the higher energies. All the four predictions are flavor independent.

It is important to note that the difference between the predictions for the neutrino and antineutrino induced reactions on each nucleus comes solely from the replacement of V_{ij} functions from Eq. (2.33) by the \bar{V}_{ij} functions defined in Eq. (2.34). In turn, the difference between the predictions for the $\nu_l + {}^3\text{He} \rightarrow \nu_l + {}^3\text{He}$ and $\nu_l + {}^3\text{H} \rightarrow \nu_l + {}^3\text{H}$ reactions is caused nearly exclusively by the proton (j_{NC}^p) and neutron (j_{NC}^n) contributions in the following isospin matrix element:

$$\mathcal{I}(t, m_T) \equiv \left\langle \left(t \frac{1}{2} \right) \frac{1}{2} m_T \mid \frac{1}{2} (1 + \tau_z(1)) j_{NC}^p + \frac{1}{2} (1 - \tau_z(1)) j_{NC}^n \mid \left(t \frac{1}{2} \right) \frac{1}{2} m_T \right\rangle, \quad (4.1)$$

which yield in the ${}^3\text{He}$ case ($m_T = \frac{1}{2}$) $\mathcal{I}(0, \frac{1}{2}) = j_{NC}^p$, $\mathcal{I}(1, \frac{1}{2}) = \frac{2}{3}j_{NC}^n + \frac{1}{3}j_{NC}^p$, and in the ${}^3\text{H}$ case ($m_T = -\frac{1}{2}$) $\mathcal{I}(0, -\frac{1}{2}) = j_{NC}^n$, $\mathcal{I}(1, -\frac{1}{2}) = \frac{2}{3}j_{NC}^p + \frac{1}{3}j_{NC}^n$. The differences introduced by the slightly different masses and wave functions of ${}^3\text{He}$ and ${}^3\text{H}$ are practically negligible. The same is also true for the two antineutrino induced elastic reactions.

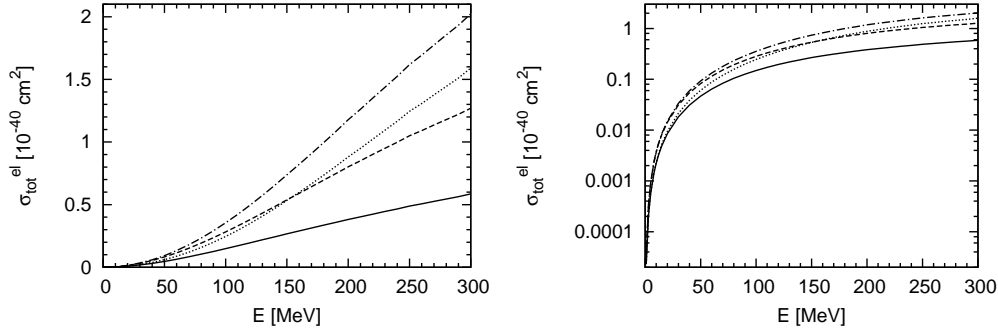


FIG. 14. The total cross section for the elastic NC driven reactions $\bar{\nu}_l + {}^3\text{He} \rightarrow \bar{\nu}_l + {}^3\text{He}$ (solid line), $\bar{\nu}_l + {}^3\text{H} \rightarrow \bar{\nu}_l + {}^3\text{H}$ (dashed line), $\nu_l + {}^3\text{He} \rightarrow \nu_l + {}^3\text{He}$ (dotted line) and $\nu_l + {}^3\text{H} \rightarrow \nu_l + {}^3\text{H}$ (dash-dotted line) as a function of the initial (anti)neutrino energy E shown on a linear (left panel) and a logarithmic (right panel) scale. The results are obtained with the AV18 NN potential and the single nucleon NC operator, which contains the relativistic corrections.

The CC and NC driven break-up reactions are definitely more demanding than the formerly discussed ones due to the complicated kinematics, which has to take into account two- and three-body disintegration processes. Full inclusion of the final state interactions is even more challenging, especially for the isospin raising reactions induced by the neutrinos, for which two or three outgoing nucleons are charged.

In the studies of electron scattering on the trinucleons one usually assumes that the initial electron energy, the electron scattering angle and the final electron energy are known. This information allows one to study the 3N scattering states at a fixed 3N internal energy and at a fixed total 3N momentum. In the case of the (anti)neutrino induced processes one is interested predominantly in the total cross sections, which necessitates a calculation of at least hundreds of the neutrino kinematics. Even for the (anti)neutrino reactions with the deuteron calculations are indeed time consuming.

It is then important to realize that the essential dynamical quantities for inclusive reactions, the so-called response functions R_i , depend on two parameters only. These parameters are the energy transfer ω and the magnitude of the three-momentum transfer $Q \equiv |\mathbf{Q}|$. We show in Fig. 15 the ranges of these quantities for the NC neutrino inelastic scattering for the initial (anti)neutrino energy $E = 100$ MeV. Of course the same statement is true also for the CC induced reactions, so in both cases the total cross sections are built from the purely kinematical input and the response functions, calculated in the whole physical ω - Q region.

The response functions $R_i \equiv R_i(\omega, Q)$ stem from various products of the nuclear matrix elements: $R_{00} \propto |N^0|^2$, $R_{ZZ} \propto |N_z|^2$, $R_{MM} \propto |N_{-1}|^2$, $R_{Z0} \propto \text{Re}(N^0(N_z)^*)$ and $R_{PP} \propto |N_{+1}|^2$, receiving contributions from all the final nuclear states. Using the approach described in Eq. (2.52), these contributions can be separately calculated for the two values of the total 3N isospin, $T = \frac{1}{2}$ and $T = \frac{3}{2}$. On the other hand the same sum over the final nuclear states can be performed over the physical two-body and three-body fragmentation channels. An agreement between these two approaches provides a non-trivial test of numerics.

In this work we restrict ourselves to a sample of results for the CC and NC response functions. They are calculated for the fixed value of the three-momentum transfer $Q = 100$ MeV/c, as a function of the internal 3N energy $E_{c.m.}$. The latter quantity is simply related

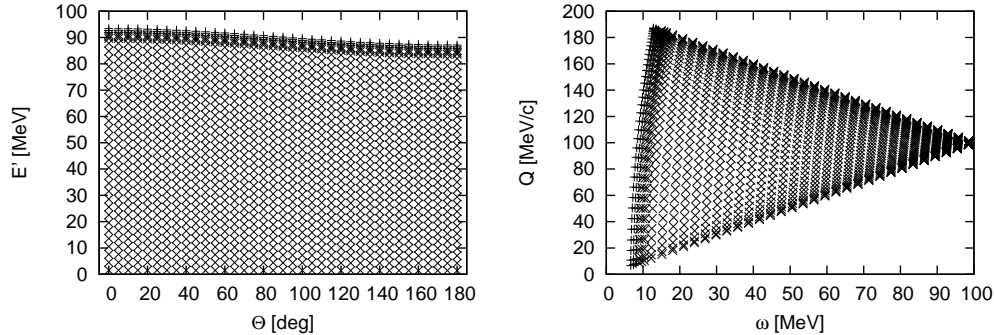


FIG. 15. The ranges of various kinematical quantities describing the kinematics of the NC driven break-up of ${}^3\text{H}$ for the initial (anti)neutrino energy $E=100$ MeV. In the left panel the outgoing (anti)neutrino energy and the scattering angle are considered, while in the right panel the magnitude of the three-momentum transfer is plotted versus the energy transfer.

to the energy transfer. For example, in the case of the antineutrino CC break-up of ${}^3\text{H}$ it reads

$$E_{c.m.} = \omega + M_{3H} - 3M_n - \frac{Q^2}{6M_n}, \quad (4.2)$$

where the M_{3H} and M_n are the triton and neutron masses, respectively.

The five inclusive CC response functions $R_{i,CC}$ for the electron antineutrino disintegration of ${}^3\text{He}$ are shown in Fig. 16. They all have a very similar shape, known also from inclusive electron-nucleus scattering (see for example Ref. [83]): they start from zero at threshold, rise to reach a maximum, whose position corresponds to antineutrino scattering elastically from a moving bound nucleon, and slowly tend to zero for higher $E_{c.m.}$ values. In Fig. 16 we show also separate contributions from the total isospin $T = \frac{1}{2}$ states (dotted line) and from the two-body break-up channel (dashed line), while the total response function is computed either as a sum of the $T = \frac{1}{2}$ and $T = \frac{3}{2}$ parts (dash-dotted line) or as a sum over the two- and three-body break-up contributions (solid line). As expected, for each R_i the dash-dotted and solid lines overlap and the relative distance between the solid and dotted lines provides information about the importance of the $T = \frac{3}{2}$ (present only in the three-body break-up) contribution. The corresponding difference between the solid and dashed lines provides information about the contribution to the total response function from the three-body break-up channel.

In the same way we display the inclusive NC response functions $R_{i,NC}$ for the (anti)neutrino disintegration of ${}^3\text{H}$ in Fig. 17 and for the (anti)neutrino disintegration of ${}^3\text{He}$ in Fig. 18. These response functions are the same for the neutrino and antineutrino induced reactions. From Figs. 17 and 18 we infer that both the $T = \frac{3}{2}$ and the three-body break-up contributions to the inclusive NC response functions are relatively much more important than for the CC response functions. Our predictions for the (anti)neutrino disintegration of ${}^3\text{He}$ suffer from the lack of Coulomb force in the calculations of the final nuclear states. Our experience from investigations of electron scattering on ${}^3\text{He}$ tells us, however, that the Coulomb force does not substantially affect *inclusive* response functions. Within our present framework we cannot describe CC neutrino induced processes with three protons in the final state.

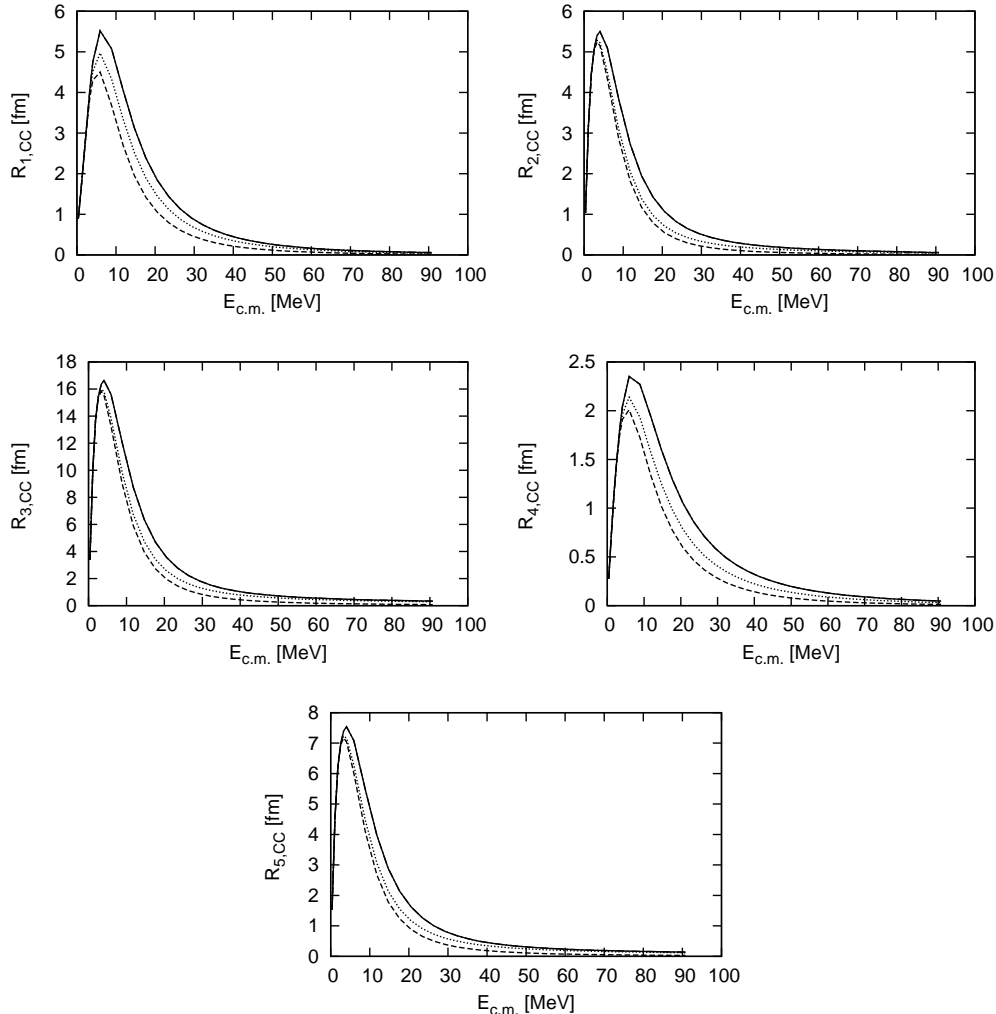


FIG. 16. The inclusive CC response functions $R_{i,CC}$ for the electron antineutrino disintegration of ${}^3\text{He}$ as a function of the internal 3N energy $E_{c.m.}$ for the fixed value of the three-momentum transfer $Q=100$ MeV/c. The results are obtained with the AV18 NN potential and the single nucleon CC operator, which contains the relativistic corrections. The dotted line shows the contribution from final nuclear states with the total isospin $T = \frac{1}{2}$ and the dash-dotted line represents the total response function obtained from the total isospin $T = \frac{1}{2}$ and $T = \frac{3}{2}$ states. The dashed line depicts the part of the response function stemming from the two-body break-up channel and the solid line the total response function, receiving contributions from both two- and three-body break-up states. Note that the dash-dotted and solid lines overlap.

V. SUMMARY AND CONCLUSIONS

A consistent framework for the calculations of several neutrino induced processes on ${}^2\text{H}$, ${}^3\text{He}$, ${}^3\text{H}$ and other light nuclei is still a challenge, despite the recent progress in this field. There are many models of the nuclear interactions and weak current operators linked to these forces, but full compatibility has not been achieved yet. The work on the regularization of the chiral potentials and electroweak current operators is in progress and the crucial issue

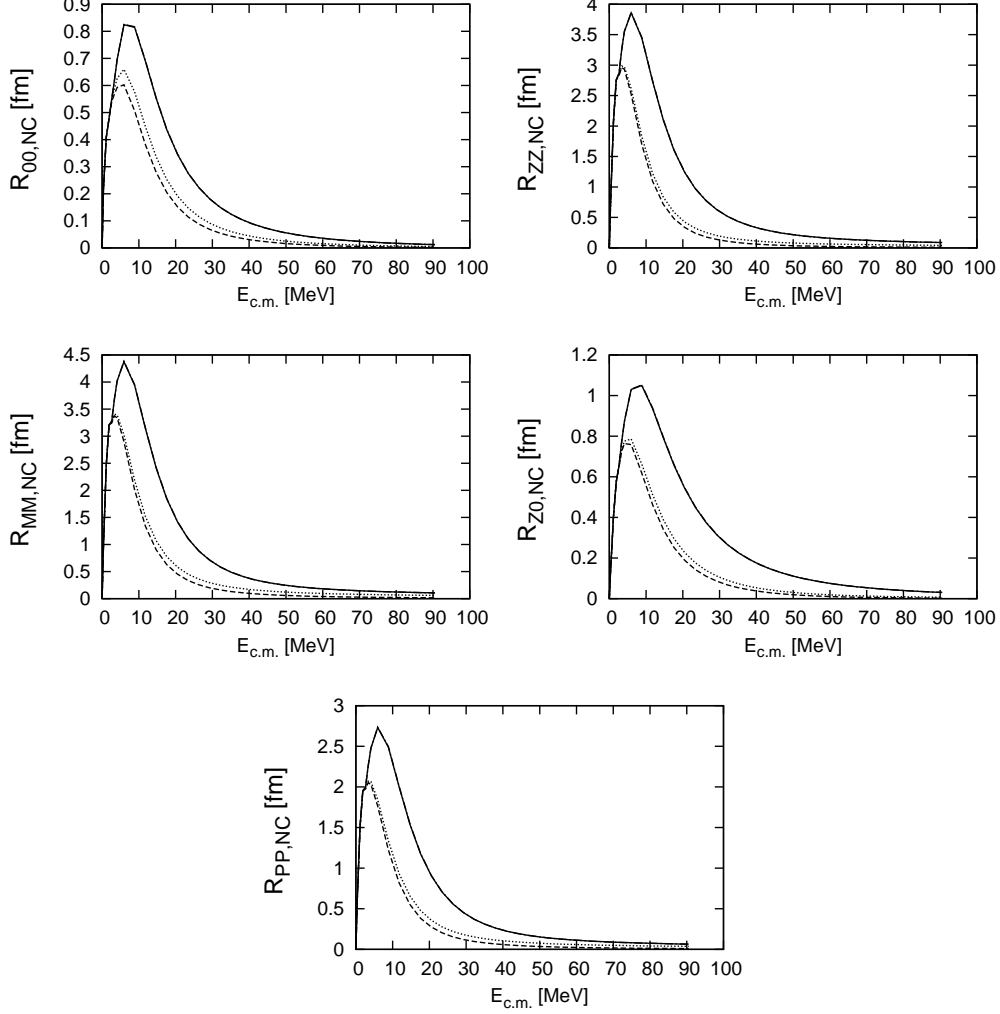


FIG. 17. The inclusive NC response functions $R_{i,NC}$ for the (anti)neutrino disintegration of ${}^3\text{H}$ as a function of the internal 3N energy $E_{c.m.}$ for the fixed value of the three-momentum transfer $Q=100$ MeV/c. The results are obtained with the AV18 NN potential and the single nucleon NC operator, which contains the relativistic corrections. Lines as in Fig. 16.

of the current conservation has to be ultimately solved. Additional problems arise from the fact that (anti)neutrinos can transfer a lot of energy and three-momentum to the nuclear system which requires a relativistic treatment of both kinematics and dynamics.

In the present paper we studied the two-nucleon $\bar{\nu}_e + {}^2\text{H} \rightarrow e^+ + n + n$, $\nu_e + {}^2\text{H} \rightarrow e^- + p + p$, $\bar{\nu}_l + {}^2\text{H} \rightarrow \bar{\nu}_l + {}^2\text{H}$, $\nu_l + {}^2\text{H} \rightarrow \nu_l + {}^2\text{H}$, $\bar{\nu}_l + {}^2\text{H} \rightarrow \bar{\nu}_l + p + n$, $\nu_l + {}^2\text{H} \rightarrow \nu_l + p + n$ and three-nucleon $\bar{\nu}_e + {}^3\text{He} \rightarrow e^+ + {}^3\text{H}$, $\bar{\nu}_l + {}^3\text{He} \rightarrow \bar{\nu}_l + {}^3\text{He}$, $\nu_l + {}^3\text{He} \rightarrow \nu_l + {}^3\text{He}$, $\bar{\nu}_l + {}^3\text{H} \rightarrow \bar{\nu}_l + {}^3\text{H}$, $\nu_l + {}^3\text{H} \rightarrow \nu_l + {}^3\text{H}$, $\bar{\nu}_e + {}^3\text{He} \rightarrow e^+ + n + d$, $\bar{\nu}_e + {}^3\text{He} \rightarrow e^+ + n + n + p$, $\bar{\nu}_l + {}^3\text{He} \rightarrow \bar{\nu}_l + p + d$, $\bar{\nu}_l + {}^3\text{He} \rightarrow \bar{\nu}_l + p + p + n$, $\nu_l + {}^3\text{H} \rightarrow \nu_l + n + d$ and $\nu_l + {}^3\text{H} \rightarrow \nu_l + n + n + p$ reactions in the framework close to the one of Ref. [8] but with the single nucleon current operator. For most of the reactions we provided predictions for the total cross sections. In the case of the (anti)neutrino- ${}^3\text{He}$ and (anti)neutrino- ${}^3\text{H}$ inelastic scattering we computed examples of the essential response functions.

The bulk of our results was obtained for the reactions with the deuteron. Here, contrary

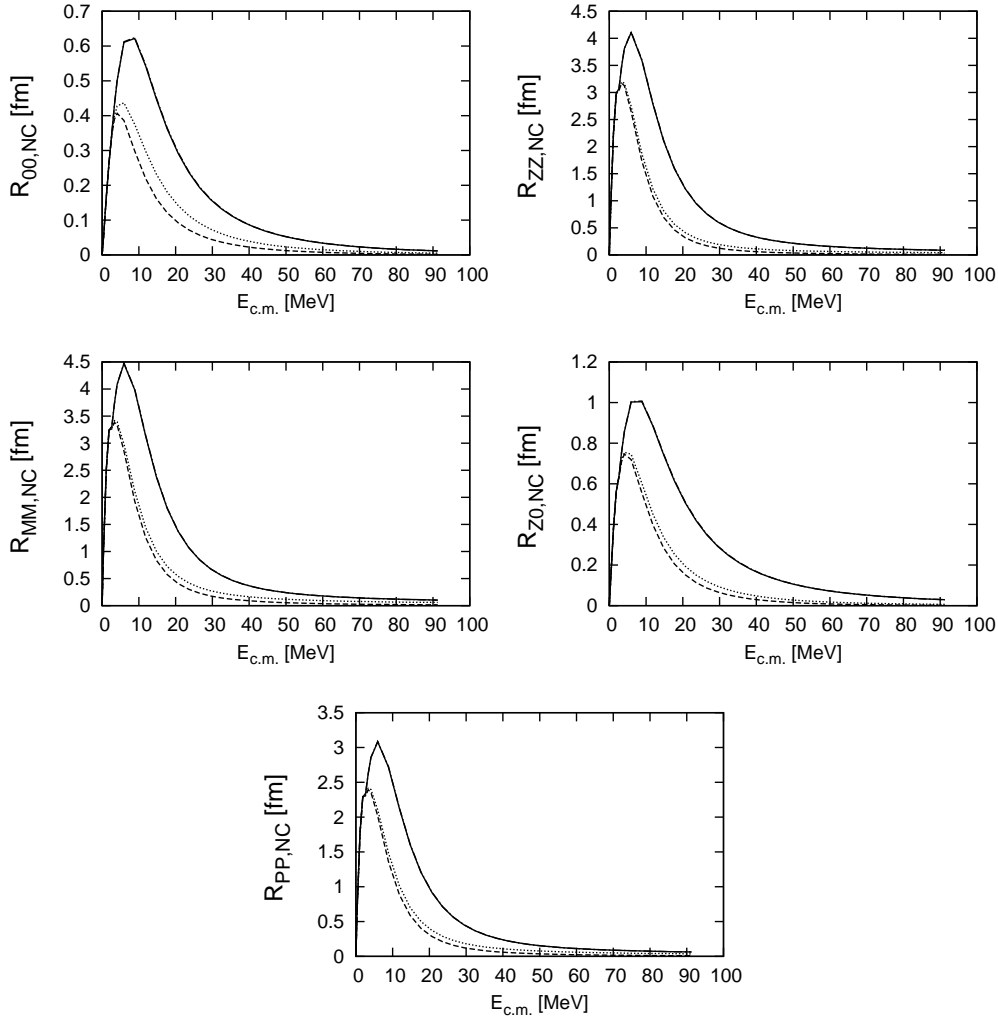


FIG. 18. The same as in Fig. 17 for the (anti)neutrino disintegration of ${}^3\text{He}$.

to Ref. [8], we restricted ourselves to the lower (anti)neutrino energies, where the use of our purely nonrelativistic approach is better justified. But even in this more restricted range of neutrino energies relativistic effects in the kinematics were thoroughly checked with the result that the main difference between the relativistic and nonrelativistic kinematics stemmed from the form of the phase space factor. We worked exclusively in momentum space, treating also the Coulomb interaction between the two outgoing protons in the form of a sharply cut off potential. This is justified because current matrix elements become negligible for sufficiently large distances between two nucleons. Last but not least, very important elements of the formalism - $2N$ scattering states in the partial wave representation - were cross-checked using the results from the momentum and coordinate space calculations.

The full understanding of the studied (anti)neutrino induced processes requires the inclusion of at least $2N$ contributions to the nuclear current operators and, especially at larger (anti)neutrino energies, consistent relativistic treatment of kinematics and dynamics. Note that momentum space offers an easier possibility to use the so-called “boosted potential”, which has been already employed in various relativistic studies of few-nucleon systems [63–69]. We plan to work along this line and perform more complete calculations in the near

future, ultimately with chiral dynamical input. We believe, however, that the predictions presented here can serve as an important benchmark.

ACKNOWLEDGMENTS

This work is a part of the LENPIC project and was supported by the Polish National Science Center under Grants No. 2016/22/M/ST2/00173 and 2016/21/D/ST2/01120. The numerical calculations were partially performed on the supercomputer cluster of the JSC , Jülich, Germany.

-
- [1] K. Kubodera and S. Nozawa, *Int. J. Mod. Phys. E* **3**, 101 (1994).
 - [2] S. Nakamura, T. Sato, V. Gudkov, and K. Kubodera, *Phys. Rev. C* **63**, 034617 (2001); Erratum: [*Phys. Rev. C* **73**, 049904 (2006)].
 - [3] S. Nakamura *et al.*, *Nucl. Phys.* **A707**, 561 (2002); <http://www-nuclth.phys.sci.osaka-u.ac.jp/top/Netal/total/index.html>.
 - [4] J. Carlson and R. Schiavilla, *Rev. Mod. Phys.* **70**, 743 (1998).
 - [5] R.B. Wiringa, V.G.J. Stoks, and R. Schiavilla, *Phys. Rev. C* **51**, 38 (1995).
 - [6] R. Machleidt, *Phys. Rev. C* **63**, 024001 (2001).
 - [7] Q.R. Ahmad *et al.* (SNO Collaboration), *Phys. Rev. Lett.* **89**, 011301 (2002); S.N. Ahmed *et al.* (SNO Collaboration), *Phys. Rev. Lett.* **92**, 181301 (2004).
 - [8] G. Shen, L. E. Marcucci, J. Carlson, S. Gandolfi, and R. Schiavilla, *Phys. Rev. C* **86**, 035503 (2012).
 - [9] M. Butler, J.-W. Chen, and X. Kong, *Phys. Rev. C* **63**, 035501 (2001).
 - [10] S. Weinberg, *Phys. Lett.* **B251**, 288 (1990).
 - [11] S. Weinberg, *Nucl. Phys.* **B363**, 3 (1991).
 - [12] E. Epelbaum, W. Glöckle, and U.-G. Meißner, *Nucl. Phys. A* **637**, 107 (1998); **671**, 295 (2000).
 - [13] E. Epelbaum, W. Glöckle, and U.-G. Meißner, *Eur. Phys. J.* **A19**, 125 (2004).
 - [14] E. Epelbaum, W. Glöckle, and U.-G. Meißner, *Nucl. Phys.* **A747**, 362 (2005).
 - [15] E. Epelbaum *et al.*, *Phys. Rev. C* **66**, 064001 (2002).
 - [16] E. Epelbaum, *Prog. Part. Nucl. Phys.* **57**, 654 (2006).
 - [17] V. Bernard, E. Epelbaum, H. Krebs, and U.-G. Meißner, *Phys. Rev. C* **77**, 064004 (2008).
 - [18] V. Bernard, E. Epelbaum, H. Krebs, and U.-G. Meißner, *Phys. Rev. C* **84**, 054001 (2011).
 - [19] E. Epelbaum, *Eur. Phys. J.* **A34**, 197 (2007).
 - [20] H. Krebs and E. Epelbaum, *Few Body Syst.* **50**, 295 (2011).
 - [21] H. Krebs, A. M. Gasparyan, and E. Epelbaum, arXiv:1803.09613 [nucl-th].
 - [22] E. Epelbaum, H. Krebs, and U.-G. Meißner, *Eur. Phys. J.* **A51**, 26 (2015).
 - [23] E. Epelbaum, H. Krebs, and U.-G. Meißner, *Phys. Rev. Lett.* **115**, 122301 (2015).
 - [24] S. Binder, A. Calci, E. Epelbaum, R. J. Furnstahl, J. Golak, K. Hebeler, H. Kamada, H. Krebs, J. Langhammer, S. Liebig, P. Maris, U.-G. Meißner, D. Minossi, A. Nogga, H. Potter, R. Roth, R. Skibiński, K. Topolnicki, J. P. Vary, and H. Witała, *Phys. Rev. C* **93**, 044002 (2016).
 - [25] R. Skibiński, J. Golak, K. Topolnicki, H. Witała, E. Epelbaum, H. Krebs, H. Kamada, U.-G. Meißner, and A. Nogga, *Phys. Rev. C* **93**, 064002 (2016).

- [26] P. Reinert, H. Krebs, and E. Epelbaum, arXiv:1711.08821 [nucl-th].
- [27] R. Navarro Pérez, J. E. Amaro, and E. Ruiz Arriola, Phys. Rev. **C88**, 064002 (2013); Erratum: [Phys. Rev. **C91**, 029901 (2015)].
- [28] S. Kölling, E. Epelbaum, H. Krebs, and U.-G. Meißner, Phys. Rev. **C80**, 045502 (2009).
- [29] S. Kölling, E. Epelbaum, H. Krebs, and U.-G. Meißner, Phys. Rev. **C84**, 054008 (2011).
- [30] H. Krebs, E. Epelbaum, and U.-G. Meißner, Ann. Phys. **378**, 317 (2017).
- [31] D. Rozpędzik, J. Golak, S. Kölling, E. Epelbaum, R. Skibiński, H. Witała, and H. Krebs, Phys. Rev. **C83**, 064004 (2011).
- [32] R. Skibiński, J. Golak, D. Rozpędzik, K. Topolnicki, and H. Witała, Acta Phys. Polon. **B46**, 159 (2015).
- [33] D. R. Entem and R. Machleidt, Phys. Rev. **C68**, 041001(R), (2003).
- [34] R. Machleidt and D.R. Entem, Phys. Rept. **503**, 1 (2011).
- [35] D. R. Entem, R. Machleidt, and Y. Nosyk, Phys. Rev. **C96**, 024004 (2017).
- [36] T.-S. Park, D.-P. Min, and M. Rho, Phys. Rep. **233**, 341 (1993).
- [37] T.-S. Park, D.-P. Min, and M. Rho, Nucl. Phys. A **596**, 515 (1996).
- [38] S. Pastore, R. Schiavilla, and J.L. Goity, Phys. Rev. C **78**, 064002 (2008).
- [39] S. Pastore, L. Girlanda, R. Schiavilla, M. Viviani, and R.B. Wiringa, Phys. Rev. C **80**, 034004 (2009).
- [40] S. Pastore, L. Girlanda, R. Schiavilla, and M. Viviani, Phys. Rev. C **84**, 024001 (2011).
- [41] A. Baroni, L. Girlanda, S. Pastore, R. Schiavilla, and M. Viviani, Phys. Rev. C **93**, 015501 (2016); **93**, 049902(E) (2016); **95**, 059901(E) (2017).
- [42] M. Piarulli, L. Girlanda, L.E. Marcucci, S. Pastore, R. Schiavilla, and M. Viviani, Phys. Rev. C **87**, 014006 (2013).
- [43] D. Gazit, S. Quaglioni, and P. Navratil, Phys. Rev. Lett. **103**, 102502 (2009).
- [44] A. Baroni, L. Girlanda, A. Kievsky, L.E. Marcucci, R. Schiavilla, and M. Viviani, Phys. Rev. C **94**, 024003 (2016); **95**, 059902(E) (2017).
- [45] T.-S. Park, L.E. Marcucci, R. Schiavilla, M. Viviani, A. Kievsky, S. Rosati, K. Kubodera, D.-P. Min, and M. Rho, Phys. Rev. C **67**, 055206 (2003).
- [46] L. E. Marcucci, R. Schiavilla, and M. Viviani, Phys. Rev. Lett. **110**, 192503 (2013).
- [47] D. Gazit, Phys. Lett. **B666**, 472 (2008).
- [48] L. E. Marcucci, M. Piarulli, M. Viviani, L. Girlanda, A. Kievsky, S. Rosati, and R. Schiavilla, Phys. Rev. **C83**, 014002 (2011).
- [49] L. E. Marcucci, A. Kievsky, S. Rosati, R. Schiavilla, and M. Viviani, Phys. Rev. Lett. **108**, 052502 (2012).
- [50] L. E. Marcucci and R. Machleidt, Phys. Rev. **C90**, 054001 (2014).
- [51] A. Baroni and R. Schiavilla, Phys. Rev. **C96**, 014002 (2017).
- [52] D. Gazit and N. Barnea, Phys. Rev. **C70**, 048801 (2004).
- [53] D. Gazit and N. Barnea, Phys. Rev. Lett. **98**, 192501 (2007).
- [54] E. O'Connor, D. Gazit, C. J. Horowitz, A. Schwenk, and N. Barnea, Phys. Rev. **C75**, 055803 (2007).
- [55] D. Efros, W. Leidemann, and G. Orlandini, Phys. Lett. **B338**, 130 (1994).
- [56] N. Barnea, W. Leidemann, and G. Orlandini, Phys. Rev. **C61**, 054001 (2000); Nucl. Phys. **A693**, 565 (2001).
- [57] N. Barnea and A. Novoselsky, Ann. Phys. (NY) **256**, 192 (1997).
- [58] A. Lovato, S. Gandolfi, J. Carlson, S.C. Pieper, and R. Schiavilla, Phys. Rev. Lett. **112**, 182502 (2014).

- [59] A. Lovato, S. Gandolfi, J. Carlson, S.C. Pieper, and R. Schiavilla, Phys. Rev. C**91**, 062501(R) (2015).
- [60] A.S. Meyer, M. Betancourt, R. Gran, and R.J. Hill, Phys. Rev. D **93**, 113015 (2016).
- [61] K. Topolnicki, J. Golak, R. Skibiński, A.E. Elmeshneb, W. Glöckle, A. Nogga, and H. Kamada, Few Body Syst. **54**, 2233 (2013).
- [62] J. Golak, R. Skibiński, H. Witała, K. Topolnicki, A. E. Elmeshneb, H. Kamada, A. Nogga, and L. E. Marcucci, Phys. Rev. C**90**, 024001 (2014).
- [63] H. Kamada, W. Glöckle, J. Golak, and Ch. Elster, Phys. Rev. C**66**, 044010 (2002).
- [64] H. Witała, J. Golak, W. Glöckle, and H. Kamada, Phys. Rev. C**71**, 054001 (2005).
- [65] J. Golak, R. Skibiński, H. Witała, W. Glöckle, A. Nogga, and H. Kamada, Acta Phys. Polon. B**38**, 2143 (2006).
- [66] T. Liu, Ch. Elster, W. N. Polyzou, H. Witała, and W. Glöckle, Phys. Rev. C**78**, 024002 (2008).
- [67] H. Witała, J. Golak, R. Skibiński, W. Glöckle, H. Kamada, and W. Polyzou, Phys. Rev. C**83**, 044001 (2011); Erratum: [Phys. Rev. C**88**, 069904 (2013)].
- [68] W. N. Polyzou, Y. Huang, Ch. Elster, W. Glöckle, J. Golak, R. Skibiński, H. Witała, and H. Kamada, Few Body Syst. **49**, 129 (2011).
- [69] W. N. Polyzou and Ch. Elster, J. Phys. G**41**, 094006 (2014).
- [70] J. Golak, R. Skibiński, H. Witała, K. Topolnicki, H. Kamada, A. Nogga, and L. E. Marcucci, Phys. Rev. C**94**, 034002 (2016).
- [71] J.D. Walecka, *Theoretical Nuclear and Subnuclear Physics*, Oxford University Press, New York, 1995.
- [72] J.D. Bjorken and S.D. Drell, *Relativistic Quantum Mechanics*, McGraw-Hill Science/Engineering/Math, 1998.
- [73] C. Lanczos, Journal of Mathematics and Physics **17**, 123 (1938).
- [74] C. de Boor and B. Swartz, SIAM J. Numer. Anal. **10**, 582 (1973).
- [75] N. W. Schellingerhout, *Factorizability in the Numerical Few-Body Problem*, Ph.D. thesis, Rijksuniversiteit Groningen, The Netherlands, 1995, ISBN 90-9008718-4.
- [76] E. Fermi, Zeitschrift für Physik **88**, 161 (1934).
- [77] A. Nogga, D. Hüber, H. Kamada, and W. Glöckle, Phys. Lett B**409**, 19 (1997).
- [78] S. Ishikawa, J. Golak, H. Witała, H. Kamada, W. Glöckle, and D. Hüber, Phys. Rev. C**57**, 39 (1998).
- [79] J. Golak, R. Skibiński, H. Witała, W. Glöckle, A. Nogga, and H. Kamada, Phys. Rept. **415**, 89 (2005).
- [80] D. Hüber, H. Kamada, H. Witała, and W. Glöckle, Acta Phys. Pol. B**28**, 1677 (1997).
- [81] T. Frederico, E. M. Henley, S. J. Pollock, and S. Ying, Phys. Rev. C**46**, 347 (1992).
- [82] M. Butler and Jiunn-Wei Chen, Nucl. Phys. A**675**, 575 (2000).
- [83] O. Benhar, D. Day, and I. Sick, Rev. Mod. Phys. **80**, 189 (2008).